Title

Rostro-Caudal Specificity of Corticospinal Tract Projections in Mice.

Journal

Cerebral Cortex, 31(5)

ISSN

1047-3211

Authors

Steward, Oswald
Yee, Kelly M
Metcalfe, Mariajose
et al.

Publication Date

2021-03-31

DOI

10.1093/cercor/bhaa338

Peer reviewed

OXFORD

Cerebral Cortex, May 2021;31: 2322–2344

doi: 10.1093/cercor/bhaa338
Advance Access Publication Date: 22 December 2020
Original Article

ORIGINAL ARTICLE

Rostro-Caudal Specificity of Corticospinal Tract Projections in Mice

Oswald Steward[1,2,3,4], Kelly M. Yee[1,2], Mariajose Metcalfe[1,2], Rafer Willenberg[1,2,6], Juan Luo[5], Ricardo Azevedo[3], Jacob H. Martin-Thompson[3] and Sunil P. Gandhi[3]

[1]Reeve-Irvine Research Center, University of California Irvine, Irvine, CA 92697, USA, [2]Department of Anatomy & Neurobiology, University of California Irvine, Irvine, CA 92697, USA, [3]Department of Neurobiology & Behavior, University of California Irvine, Irvine, CA 92697, USA, [4]Department of Neurosurgery, University of California Irvine, Irvine, CA 92697, USA, [5]Department of Physiology, Tongji Medical College, Huazhong University of Science and Technology, Wuhan, China and [6]Current address: Department of Neurology, Cedars-Sinai Medical Center, Los Angeles, CA 90048, USA

Address correspondence to Oswald Steward, University of California Irvine, 1101 GNRF, 837 Health Sciences Dr, Irvine, CA 92697, USA.
Email: osteward@uci.edu

Abstract

Rostro-caudal specificity of corticospinal tract (CST) projections from different areas of the cortex was assessed by retrograde labeling with fluorogold and retrograde transfection following retro-AAV/Cre injection into the spinal cord of tdT reporter mice. Injections at C5 led to retrograde labeling of neurons throughout forelimb area of the sensorimotor cortex and a region in the dorsolateral cortex near the barrel field (S2). Injections at L2 led to retrograde labeling of neurons in the posterior sensorimotor cortex (hindlimb area) but not the dorsolateral cortex. With injections of biotinylated dextran amine (BDA) into the main sensorimotor cortex (forelimb region), labeled axons terminated selectively at cervical levels. With BDA injections into caudal sensorimotor cortex (hindlimb region), labeled axons passed through cervical levels without sending collaterals into the gray matter and then elaborated terminal arbors at thoracic sacral levels. With BDA injections into the dorsolateral cortex near the barrel field, labeled axons terminated at high cervical levels. Axons from medial sensorimotor cortex terminated primarily in intermediate laminae and axons from lateral sensorimotor cortex terminated primarily in laminae III–V of the dorsal horn. One of the descending pathways seen in rats (the ventral CST) was not observed in most mice.

Significance
Mice are used extensively for studies of regeneration following spinal cord injury because of the ability to create genetic modifications to explore ways to enhance repair and enable axon regeneration. A particular focus has been the corticospinal tract (CST) because of its importance for voluntary motor function. Here, we document features of the rostro-caudal specificity of CST projections.

Key words: biotinylated dextran amine, mouse, retro-AAV, sensorimotor cortex, spinal cord

Introduction

Mice are used extensively for studies of regeneration following spinal cord injury because of the ability to create genetic modifications to explore the role of particular genes in regulating or enabling axon regeneration (Zheng et al. 2006). Regeneration of the corticospinal tract (CST) has been of particular interest because of the key role the CST plays in controlling voluntary motor function. Recent studies have documented that several different genetic manipulations can enable regeneration of CST axons past a spinal cord injury (Liu et al. 2010; Du et al. 2015; Wang et al. 2015; Hollis et al. 2016) and/or promote sprouting of uninjured CST axons after partial injury (Geoffroy et al. 2015).

One question that has not been addressed in most studies is the degree to which regenerated CST axons recapitulate normal specificities of projection. For example, do the CST axons that extend past a cervical level injury originate from neurons that normally project to cervical levels or are they axons that normally project to lumbar and sacral levels? The answer is important for interpreting recovery of motor function and cortical remapping that occurs in conjunction with regenerative growth (see for example Hollis et al. 2016).

Addressing questions about rostro-caudal specificity of regenerated CST axons and interpreting accompanying recovery of motor function requires an understanding of normal CST projection specificity. In this regard, some aspects of projection specificity to spinal levels (C7 vs. L4) have been explored (Kamiyama et al. 2015), but details of projection specificity from different parts of the sensorimotor cortex have not been extensively explored in mice.

The primary goal of the present study was to map the rostro-caudal projection patterns from different parts of the sensorimotor cortex to the spinal cord in mice. We were especially interested in determining whether CST axons that project from hindlimb cortex to lumbosacral sections also gave rise to collaterals at cervical levels and whether CST axons from forelimb regions also extended axons to lumbar levels. Another aspect of CST organization that is not well understood is the pattern of projection of neurons outside the main sensorimotor cortex. Injections of retrograde tracers into the cervical spinal cord of rats lead to retrograde labeling of pyramidal neurons in the rostral forelimb area (RFA) and in an area in the dorsolateral neocortex cortex near the barrel field (Nielson et al. 2010), but projection patterns of neurons in these regions are unknown. The other aspect of CST organization that is not well studied is the degree of bilaterality of CST projections from different parts of the sensorimotor cortex. This is of interest because trans-midline sprouting after unilateral pyramidotomy is one of the main models for testing interventions to enhance sprouting after injury (Geoffroy et al. 2015).

Here, we assess topography of CST projections by mapping the cells of origin of CST projections and by mapping projections from different areas using BDA tract tracing. Key findings are as follows: 1) CST axons from the forelimb region of the main sensorimotor cortex terminate selectively in cervical levels without extending to thoracic levels and below; 2) axons from the caudal part of the main sensorimotor cortex (hindlimb region) extend through cervical regions to terminate in lumbar through sacral segments without extending collateral branches into the cervical gray matter; 3) the RFA in the frontal cortex and the dorsolateral neocortex near the barrel field project selectively to high cervical levels; 4) axons from the medial portion of the main sensorimotor cortex (M1) arborize primarily in the intermediate lamina with some axons extending into the ventral horn, whereas axons from the lateral portion of the main sensorimotor cortex arborize primarily in the dorsal horn; and 5) the degree of bilaterality of CST projections varies by area and level.

Methods

Experimental Animals

These studies involved mice of different strains (Table 1): male Balb/C mice, which were purchased from Harlan Labs; Rosa^{tdTomato} mice with a lox-P flanked STOP cassette that prevents expression tdTomato (obtained originally from Jackson Labs and maintained in our breeding colony for several generations); *Pten*$^{loxP/loxP}$/Rosa^{tdTomato} transgenic mice that we generated by crossing *Pten*$^{loxP/loxP}$ with Rosa^{tdTomato} mice (maintained in our breeding colony); and CST-YFP mice (Bareyre et al. 2005), which are the F1 progeny of a parental mouse with *Emx-Cre* and a mouse with *Thy1-stop-YFP* [B6.Cg-Tg(Thy1-EYFP)15Jrs/J, Jackson Labs]. Rosa^{tdTomato} mice and CST-YFP mice have a C57Bl/6 genetic background and *Pten*$^{loxP/loxP}$/Rosa^{tdTomato} transgenic mice have mixed genetic background (C57Bl/6 & 129Sv). Mice were at least 90 days of age at the time of the tracer or AAV injections. Both male and female mice were used for studies with retro-AAV.

Fluoro-Gold Injections for Retrograde Labeling

To generate a map of cortical neurons that give rise to the CST, 3 adult CST-YFP mice were injected bilaterally with a total of 0.4 µL of 4% Fluoro-Gold (Fluorochrome, LLC; Denver, CO) at cervical level 5 (C5). Mice were anesthetized with isofluorane, and the spinal cord was exposed by laminectomy at C5. Injections were made bilaterally at 0.5 mm lateral to the midline and 0.5 mm deep, with 0.2 µL injected at each site using an electronically controlled injection system (Nanoliter 2000 injector and Micro4 pump controller, World Precision Instruments) fitted with a pulled glass micropipette. One week following injections, mice were transcardially perfused with 4% paraformaldehyde in 0.1M phosphate buffer (4% PFA), and brains and spinal cords were dissected and postfixed in 4% PFA overnight before being equilibrated and stored in 27% sucrose at 4 °C.

Brains from mice injected with Fluoro-Gold were embedded by freezing in TissueTek O.C.T. (VWR International). Cryostat sections were taken in the coronal plane at 30 µm, and free-floating sections were collected in PBS at 420-µm interval through the cortex and mounted onto gelatin-coated slides. Brain sections were imaged at ×4 on an Olympus IX80 fluorescence microscope, and overlapping images were stitched together in ImageJ (Rasband, W.S., ImageJ, National Institutes of Health, http://imagej.nih.gov/ij/, 1997–2014) using linear blending fusion in the Preibisch stitching plugin (Preibisch et al. 2009).

Retrograde Transfection of Cortical Motoneurons with Retro-AAV/Cre in tdTomato Reporter Mice

To label cortical motoneurons (CMNs) in a way that allows visualization of dendritic arbors and produces labeling that is optimal for light sheet microscopy, we used AAVs that are retrogradely transported (retro-AAV) in transgenic Rosa^{tdTomato} and *Pten*$^{loxP/loxP}$/Rosa^{tdTomato} mice. In both transgenic strains, mice are homozygous for transgenes. Adult mice received bilateral injections of retro-AAV/Cre (0.3 µL each) at cervical level 5 (C5)

Table 1 The mouse strain for each experiment, AAV vector type, type of BDA used (miniruby-conjugated or unconjugated), target coordinates for injections, and animal number

Strain and number	Tracer	Target coordinates	Animal number
$Rosa^{tdTomato}$	retro-AAV/Cre	C5 ($n=4$)	0315A-H
$PTEN^{f/f}$;$Rosa^{tdTomato}$ ($n=8$)		L2 ($n=4$)	1-month survival
$Rosa^{tdTomato}$	retro-AAV/Cre	L2	0612A,B
$N=2$			3-week survival
$PTEN^{f/f}$;$Rosa^{tdTomato}$	retro-AAV/Cre at L2,	C5 and L2	0612C,D
($n=2$)	retro-AAV/shPTEN-GFP at C5		3-week survival
$Rosa^{tdTomato}$	retro-AAV/Cre	C5 ($n=8$)	0820A,B,L,M,N,O,P
$PTEN^{f/f}$;$Rosa^{tdTomato}$		L2 ($n=3$)	1-year survival
($n=11$)			
CST-YFP, $n=3$	Fluoro-Gold	C5 spinal cord 0.5L	1026C,D,E
Balb/C, $n=3$	BDA unconjugated	1.0A,1.5L	1120A,B,C
Balb/C, $n=5$	BDA miniruby	0.5A, 1.0L	0225E,F,G,H,I
Balb/C, $n=3$	BDA miniruby	1.0A, 1.0L	0225A,B,D
			0321A,B,C
Balb/C, $n=3$	BDA unconjugated	0-at bregma, 1.0L	1120D,E,F
Balb/C, $n=3$	BDA unconjugated	1.0P, 1.0L	1120G,H,I
Balb/C, $n=6$	BDA miniruby	1.0P, 1.5L	0225K,L,N,O
Balb/C, $n=6$	BDA miniruby	2.0P, 1.5L	0321F,G,H,J
Balb/C, $n=3$	BDA miniruby	2.5P, 1.5L	0225M,P,J
Balb/C, $n=3$	BDA miniruby	2.8A, 0.8L	0313A-C
Balb/C, $n=3$	BDA miniruby	1.1P, 3.2L, 1.1 deep	0408A-C
Balb/C, $n=3$	BDA unconjugated	1.0A, 2.25L	0812A-C
Balb/C, $n=3$	BDA unconjugated	0-at bregma, 2.25L	0812D-F
Balb/C, $n=3$	BDA unconjugated	1.0P, 2.25L	0812G-I

All cortical injection depths are 0.5 mm unless otherwise noted. $Rosa^{tdTomato}$ and $PTEN^{f/f}$;$Rosa^{tdTomato}$ are homozygous at both transgenic loci. Both $Rosa^{tdTomato}$ and $PTEN^{f/f}$;$Rosa^{tdTomato}$ mice are included because the accompanying PTEN deletion in $PTEN^{f/f}$;$Rosa^{tdTomato}$ mice is considered to be irrelevant for this study.

or L2 vertebral level (see Table 1 for a summary of cases included here). Mice were anesthetized with isofluorane, and the spinal cord was exposed by laminectomy at vertebral level C5 or L2. Bilateral injections were made using a Hamilton microsyringe at 0.5 mm lateral to the midline at a depth of 0.5 mm. Three to four weeks postinjection (see Table 1), mice were transcardially perfused with 4% paraformaldehyde in 0.1 M phosphate buffer (4% PFA), and brains and spinal cords were dissected, postfixed in 4% PFA overnight, and stored in buffer at 4 °C. Another set of mice received injections at C5 ($n=8$) or L2 ($n=3$) and survived for 1 year post-AAV injection to assess whether there were any negative consequences of long-term PTEN deletion via retro-AAV/Cre.

To assess whether there were populations of CMNs that could be cotransfected by retro-AAV injected into different spinal levels (C5 vs. L2), mice ($n=2$) received injections of retro-AAV/Cre into the lumbar spinal cord (L2 vertebral level) and retro-AAV/shPTEN-GFP (a vector we engineered to knock down PTEN for studies of axon regeneration in rats).

Fixation and Tissue Processing

Mice were perfused transcardially with 4% paraformaldehyde in 0.1 M phosphate buffer (4% PFA). Brains were dissected with spinal cords attached and postfixed in 4% PFA overnight. We discovered that tdT fluorescence can be easily visualized in intact brains and spinal cords by fluorescence epi-illumination. For this, brains with attached spinal cords are placed temporarily on a microscope slide and illuminated by epifluorescence (NG cube) using the 2× objective of an Olympus AX80 microscope. Images were taken at ×2 and tiled to produce a complete low power reconstruction of tdT fluorescence in the spinal cord and brain. Subsequently, brains and spinal cords were returned to PBS prior to preparation either for light sheet microscopy ($n=6$, see below) or sectioning for immunocytochemistry (all other cases).

For sectioning, brains were cryoprotected in 27% sucrose, embedded in TissueTek O.C.T. (VWR International), and frozen. Blocks were sectioned by cryostat in the coronal plane at 30 µm, and free-floating sections were collected in PBS at 480-µm interval through the cortex. One set of sections was mounted in serial order on microscope slides for visualization of native tdT fluorescence. Other sets of sections were immunostained for tdT.

Assessment of Colabeling for tdT and GFP

In mice that received injections of retro-AAV/Cre at L2 and retro-AAV/GFP at C5, we assessed colabeling of cortical neurons by immunostaining sections for GFP (FITC) and visualizing native tdT fluorescence in the same sections. For this, it was important to identify a GFP antibody that did not cross-react with the closely related tdT protein. To test for cross-reactivity, sections from mice that received AAV/Cre only were immunostained using three commercial GFP antibodies (Invitrogen, rabbit anti-GFP, catalog #A11122; Abcam, goat anti-GFP, catalog #AB6673; and Novus, rabbit anti-GFP, catalog #NB600–308). All GFP antibodies were used at a dilution of 1:1000.

Tissue Clearing and Light Sheet Fluorescence Microscopy

Six brains were processed for light sheet microscopy (2 with C5 injections and 4 with L2 injections). Brains and attached

spinal cords were immunostained and made optically transparent using a modified iDISCO+ whole-mount staining protocol (http://www.idisco.info; Renier et al., 2016). The following modifications were made to the iDISCO+ protocol: 1) The incubation step in permeabilization solution was followed by 2 additional 1-h washes with Ptx.2. Tissue was incubated in 6 mL 1:600 (10 µL) rabbit anti-RFP (Rockland, Lot# 35868) for 6 days. Secondary antibody amplification was done in 6 mL 1:600 (10 µL) Alexa Fluor 568 donkey anti-rabbit IgG (Thermo Fisher, Lot# 2044343) for 6 days.

Cleared brains were imaged on a Z.1 LSFM (Carl Zeiss Microscopy) modified for large, cleared samples in high refractive index solutions using a 5×/0.16NA detection objective. We used a commercial kit (Mesoscale Imaging System, Translucence Biosystems) to enable the Z.1 to perform deep tissue imaging. The kit provides an enlarged immersion chamber and adapted optics for high refractive index solutions allowing deep tissue imaging in dibenzyl ether (DBE).

Samples were mounted on a custom sample holder providing a sagittal view to the detection objective and submerged in DBE. Each sample was illuminated through the left optic using a 561-nm laser line paired with a BP 575–615 emission filter at 60% power and 100 ms exposure. To construct a rendering of the whole sample, multiple z-stack scans were imaged in tiles with 20% overlap. Tiles were then stitched together in Vision4D (Arivis AG), and the completed image was rendered in Imaris 9.5 (Oxford Instruments) for analysis.

Injections of Biotinylated Dextral Amine for Orthograde Tracing of CST Projections

For intracranial biotinylated dextral amine (BDA) injections, mice were anesthetized with isofluorane and positioned in a stereotaxic device. The scalp was incised at the midline and burr holes were placed in the skull overlying the right sensorimotor cortex. Injections were delivered as described below, and after the completion of the injections, the scalp was sutured and mice were placed on a water circulating heating pad at 37 °C until they regained consciousness.

Table 1 summarizes the details on intracortical injections of BDA to trace CST projections from different cortical regions. Sets of injections were made along the rostro-caudal axis of the medial part of the sensorimotor cortex (1.0–1.5 mm lateral to the midline) and laterally at 2.0–2.5 mm lateral to the midline (Fig. 1*J* for a map of injection sites). As noted, some mice received miniruby-conjugated BDA; the remainder received unconjugated BDA. Our impression was that miniruby conjugated produced less orthograde labeling than unconjugated BDA, but we did not attempt to quantify this difference. Both types of BDA were dissolved in 0.9% saline at a concentration of 10% weight/volume. Injections were made using either a Hamilton microsyringe fitted with a pulled glass micropipette or with an electronically controlled injection system (Nanoliter 2000 injector and Micro4 pump controller, World Precision Instruments). Injections were at a depth of 0.5 mm, and each individual injection was 0.4 µL delivered over the course of 3–4 min.

Mice were allowed to survive for 14 days postinjection and then were euthanized with Euthasol and perfused transcardially with 4% PFA in 0.1 M phosphate buffer. Brains and spinal cords were dissected and stored in 4% PFA and were transferred to 27% sucrose at 4 °C for cryoprotection 1 day before being frozen for sectioning.

For sectioning, the entire spinal cord was embedded in OCT, frozen, and cross-sections were taken throughout the rostro-caudal extent of the spinal cord from the spinomedullary junction through the sacral region maintaining serial order. Sections taken every 500 µm were stained for BDA. Because the spinal cord was frozen with its natural curvature (no straightening), axons in sections in areas of the curvature pass through the section at an angle rather than being perpendicular to the plane of the section.

BDA Staining

One set of floating sections through the spinal cord was stained with avidin–biotin–peroxidase; another was stained for Cy3 fluorescence. For BDA staining with avidin–biotin–peroxidase, sections were washed in PBS with 0.1% Triton X-100 3 times and then incubated overnight in avidin–biotin–peroxidase complex (Vector Laboratories, PK-6100) in PBS with 0.1% Triton X-100 at room temperature. The following day, sections were washed in PBS 3× and then stained in nickel-enhanced diaminobenzidine solution (Vector Laboratories, SK-4100) for 25 min. Sections were washed in PBS and then mounted on gelatin subbed slides, air dried, dehydrated, cleared, and then coverslipped.

For BDA staining with Cy3 amplification, sections were washed in PBS and then incubated in 1:200 dilution streptavidin-HRP (Perkin Elmer NEL75000-1ea) in PBS for 2 h, washed 3 times in PBS, and then reacted with TSA-Cy3 (1:100) in the supplied amplification diluent (Perkin Elmer SAT704A001ea). Sections were washed 2 times in PBS, then mounted on gelatin subbed slides, and coverslipped with Vectashield (Vector labs H-1000).

Image Manipulation

We discovered that the distribution of terminal arbors in the spinal cord was more evident when color images with red fluorescent axons were imported into Photoshop, converted to black and white, and inverted with auto contrast adjustment. Accordingly, all images of BDA-labeled axons are presented in this way.

Quantification of CST Axons at Different Spinal Levels

Spinal cord cross-sections taken at 500-µm interval that were stained for BDA using avidin–biotin–peroxidase were mounted in serial order on a single microscope slide. In each section, images were taken at ×60 of BDA-labeled axons in the dorsal column (dorsal CST) and dorsal part of the lateral column (dorsolateral CST). Images were imported into Photoshop, and BDA-labeled axons in each tract were counted, marking each as it was counted to avoid double counting. Counts were assembled into a Prism file and displayed as graphs of numbers of BDA-labeled CST axons at different rostro-caudal locations.

Results

Distribution of the Cells of Origin of Corticospinal Projections

Our initial approach to map the cells of origin of CST projections was done before the development of retro-AAV technology and used retrograde labeling with fluorogold (FG). The goal was to aid in defining coordinates to target populations of CST neurons within and outside of the canonical sensorimotor cortex. In mice that received bilateral injections of FG at C5, retrogradely labeled neurons were evident in the sensorimotor cortex, dorsomedial

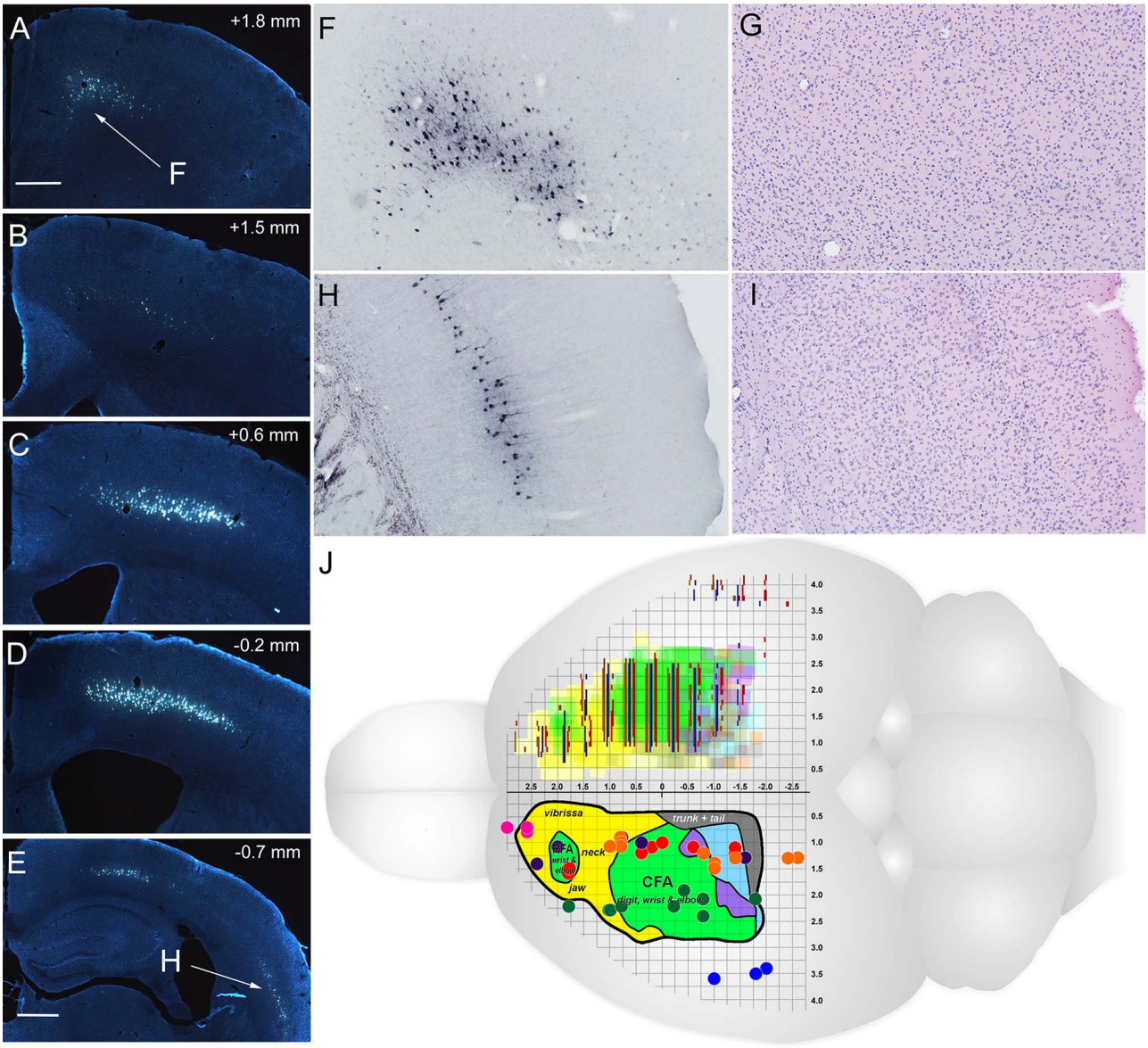

Figure 1. Rostro-caudal distribution of FG-labeled cell bodies in the cortex following injections of FG at C5. (*A–E*) Area of the cortex containing retrogradely labeled neurons at different rostro-caudal levels. Coordinates with respect to bregma are indicated in the upper right of each panel. Scale bars = 400 µm in *A* (applies to *A–D*); 400 µm in *E*. (*F*, *G*) Higher magnification view of retrogradely labeled CST neurons in the dorsomedial frontal cortex immunostained for FG and nearby section stained for cresyl violet. (*H*, *I*) Retrogradely labeled CST neurons in the dorsolateral cortex (*H*) and nearby section stained for cresyl violet. (*J*) Map of distribution of retrogradely labeled CST neurons and injection sites. Different pairs of colored lines indicate the distribution of retrogradely labeled neurons in 3 mice. Each pair of shaded colors represents the span of labeled cells on the two sides. Colored dots represent coordinates for BDA injections on a particular date represented in Figs 5–13. Some injection sites were plotted with slight offset to enable visualization of overlapping sites. *J* was created using a base drawing provided by Dr T. Jones, which is a modified version of Figure 2B in Tennant et al. (2010).

frontal cortex, and dorsolateral cortex ventral to the S1 barrel field, in a pattern similar to what is seen in rats (Nielson et al. 2011). Figure 1A–E illustrates the case with the largest number of retrogradely labeled neurons.

FG-positive neurons were evident in layer V throughout the primary motor, secondary motor, and primary somatosensory cortical areas from approximately 2.3 mm rostral to 1.5 mm caudal to bregma (Fig. 1). We refer to this hereafter as the "main sensorimotor cortex." Retrogradely labeled cells were also present in the dorsomedial frontal cortex (centered at about 2.8 mm anterior to bregma) in a region approximately 750 µm lateral to midline and approximately 600 µm deep (Fig. 1A). This area is rostral to the RFA defined in rats through microstimulation studies (Neafsey and Sievert 1982). The FG-labeled neurons in this rostral area are of approximately the same size and shape as the FG-labeled neurons in layer V in the main sensorimotor cortex. We use the term "CST neurons" to refer to all cortical neurons that give rise to CST axons and the term "cortical motoneurons" to refer to CST neurons in areas of the sensorimotor cortex in which microstimulation elicits motor responses. As in rats, there was also a spatially distinct population of FG-labeled cells in the dorsolateral cortex posterior to bregma, which also had the

typical pyramidal form characteristic of the FG-labeled neurons in layer V of the main sensorimotor cortex (Fig. 1*H*). This area was well separated from the main sensorimotor cortex by an area with few if any retrogradely labeled neurons.

Higher magnification views of retrogradely labeled CST neurons in the two areas outside the main sensorimotor cortex are illustrated in Figure 1*F*,*H* in sections immunostained for FG, and the cytoarchitecture of the regions is illustrated in nearby sections stained for cresyl violet in Figure 1*G*,*I*. Coronal sections through the dorsomedial frontal cortex are not perpendicular to the cortical surface, so cortical lamination is obscured, and the dendrites of the retrogradely labeled CST neurons extend out of the plane of the section. The area containing FG-labeled neurons in the dorsolateral cortex is just ventral to the S1 barrel field and extends caudally into S2 (Fig. 1*I*). This area has been termed "S2" (Kamiyama et al. 2015) and we will use that terminology here. Although this region has been designated as S2, it contains large neurons in layer V that appear very similar in morphology to those in the prototypical motor cortex, and are the cells of origin of CST axons.

To map the rostro-caudal distribution of retrogradely labeled cells, we identified the location of bregma based on the appearance of the sections compared with the Paxinos mouse brain atlas (Paxinos 2004). We then created a summary diagram of the distribution of FG-labeled neurons in the 3 cases by measuring the mediolateral distance over which labeled cells were found in each section and superimposed this map on a microstimulation map of cortical motor function from (Tennant et al. 2010). The mediolateral distribution of cells at different rostro-caudal locations in each mouse is represented by the different colored lines over the right hemisphere of Figure 1*J*. Overall, the area occupied by retrogradely labeled neurons overlapped with but was somewhat smaller than the motor map defined by microstimulation. The exception was the population of neurons in the dorsolateral cortex near the S1 barrel field, which is not represented in the microstimulation map.

Retro-AAV Transfection of CST Neurons in tdT Reporter Mice

Retrograde labeling via retro-AAV/Cre in tdT reporter mice has several advantages over retrograde tracing by FG. First, genetically encoded fluorescent proteins extend throughout the dendritic arbor of neurons and also into axons. Second, whereas FG might be taken up by axons that pass through an injection site (Dado et al. 1990), it has been reported that there is minimal uptake of retro-AAV by CST axons passing through the area of a spinal cord injection (Wang et al. 2018). Third, labeling produced by retrograde expression of fluorescent proteins enables imaging by light sheet microscopy, allowing global visualization of the entire population of cortical neurons that project to the spinal cord (Wang et al. 2018).

Here, we made intraspinal injections of retrograde-AAV/Cre in transgenic Rosa^{tdTomato} and *Pten*^{ff}/Rosa^{tdTomato} mice. Retrograde transfection with Cre induces biallelic expression of tdT leading to robust labeling of cell bodies, dendrites, and axons. Remarkably, tdT fluorescence can be visualized in intact spinal cords and brains by fluorescence epi-illumination without clearing (Fig. 2*A*). This provides a convenient way to document the injection site and the cloud of fluorescently labeled cortical neurons prior to sectioning or preparation for iDISCO.

In coronal sections through the brain, native tdT fluorescence can be seen without immunostaining in cell bodies and dendrites of pyramidal neurons in layer V including fine dendritic arbors in layers I–II (Fig. 2*B*,*C*). Native tdT fluorescence was most intense in nuclei. With injections at C5, tdT-positive neurons were present in the main sensorimotor cortex and in separated clusters in the dorsomedial frontal cortex and the dorsolateral cortex (S2).

With immunostaining, tdT labeling extended throughout the dendritic arbor revealing a dense network of dendrites in layers V and I/II (Fig. 2*D*). Figure 2*D* illustrates the main sensorimotor cortex and Figure 2*E* illustrates labeled neurons in the dorsolateral cortex (S2). In both sites, labeled CST neurons had a similar morphology, with a large pyramidal shaped cell body, a single thick apical dendrite extending toward the cortical surface, and extensive branches in layers I and II and multiple basal dendrites in the deep part of layer V.

3D imaging of an intact brain from a different mouse with light sheet microscopy after clearing and immunostaining with iDISCO revealed thousands of tdT-positive CST neurons in layer V throughout the primary motor, secondary motor, and primary somatosensory cortical areas (Fig. 2*G* and Supplementary Movie 0315G). Clusters of tdT-positive neurons in the dorsomedial frontal cortex and the dorsolateral cortex (S2) were separated from the main sensorimotor cortex by areas with few labeled neurons. The cell bodies of individual tdT-positive layer V neurons are easily distinguishable in the light sheet renderings (Fig. 2*H* and Supplementary Movie 0315G) along with descending axons of the CST in the subcortical white matter and internal capsule, medullary pyramid, and pyramidal decussation (Fig. 2*F*,*G*).

We used the Imaris "Spots" function to estimate the number of retrogradely labeled CST neurons in the 3D light sheet reconstructions. First, the selection box was positioned to include the area containing labeled neurons in the main sensorimotor cortex on one side. Next, tdT-positive neuronal cell bodies were segmented using the "quality" thresholding procedure to recognize labeled neuronal cell bodies but exclude artifacts and labeled dendrites. Then, artifactual hits at the surface of the brain, along blood vessels, and outside the area containing retrogradely labeled neurons were manually edited. The process was repeated on the opposite side and then for the two areas in the dorsolateral cortex with tdT-positive neurons. Figure 2*G* illustrates the above threshold hits in the 4 sampled areas with retro-AAV/Cre injections at C5. Before editing, there were 10 883, above threshold hits in the main sensorimotor cortex on the left side and 10 874 on the right. After excluding non-neuronal labeling, hits due to labeled dendrites, and scattered hits outside the sensorimotor cortex, there were 9276 labeled CST neurons on each side (the fact that the counts are identical is coincidental and reflects decisions made during the editing process). Counts in the dorsolateral cortex (S2) revealed 1534 hits on the left side and 1437 on the right before editing and 905 and 1228 labeled neurons after editing for an average of 1067 labeled CST neurons per side.

To assess the extent to which the "Spots" quality thresholding included artifacts and/or failed to detect tdT-positive neuronal cell bodies, we compared "Spots" counts with manual counts in sample areas with a moderate number of labeled neurons (the RFA on the left). Manual counts in three 150 × 150 µm areas (shaded boxes in Fig. 2*H*) yielded counts of 75, 125, and 83 tdT-positive neurons and the corresponding "Spots" fields had 72, 115, and 71 (Fig. 2*I*), which represents a difference of 4%, 8%, and 14% (average of 8.7%). Large bright fluorescent artifacts were not recognized. Similarly, close inspection in the

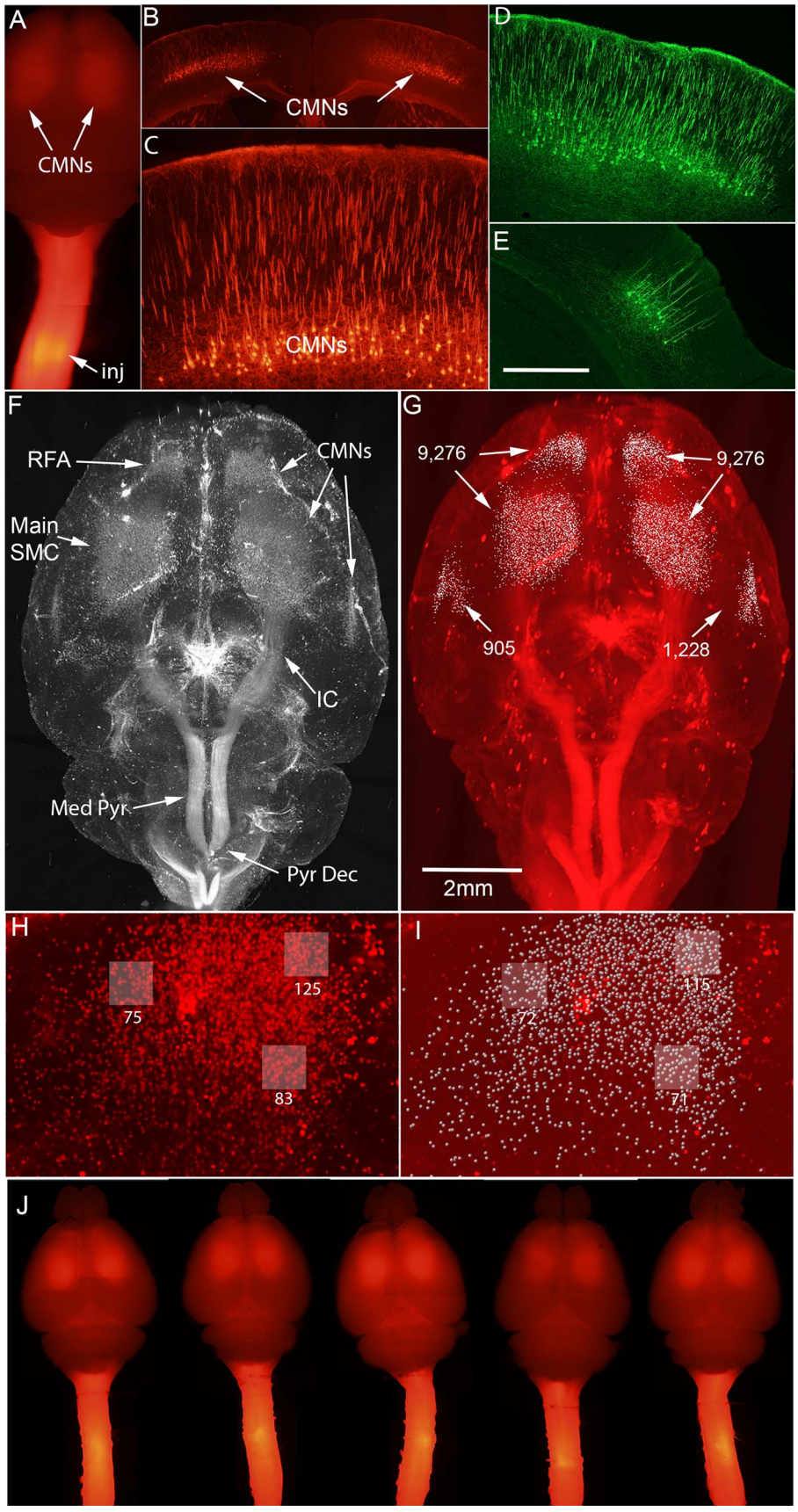

Figure 2. Retrograde transfection of cortical neurons following injections of retrograde-AAV/Cre at C5. (*A*) Visualization of tdT fluorescence in intact uncleared spinal cord and brain by fluorescence epi-illumination. (*B*) Coronal section illustrating native tdT fluorescence in cell bodies and dendrites of pyramidal neurons in layer V.

area of retrograde labeling in the main sensorimotor cortex indicates that the majority of labeled neurons were correctly recognized and few artifacts were incorrectly recognized as cells.

To illustrate the reproducibility in the pattern of retrograde transduction with the parameters used here and the persistence of expression of tdT, Figure 2*J* illustrates intact brains and spinal cords from 5 Rosa^{tdTomato} mice 1 year post-injection. These are tiled individual images taken at ×2 with epifluorescent illumination. The haze of red fluorescence indicates the constellation of neurons that are labeled and is remarkably similar across cases. One technical note is that illumination by epifluorescence is a very convenient way to screen for patterns of labeling that can be accomplished in minutes, especially because no special equipment is needed other than a standard fluorescence microscope with low power objectives.

Injections of retro-AAV/Cre into lumbar regions (L2 vertebral level) led to retrograde transduction of layer V neurons in a smaller region of the posterior sensorimotor cortex extending from about bregma to 1.8 mm posterior and from 0.8 to 1.8 mm lateral to the midline. Figure 3A–C illustrates intact brains and spinal cords from one *Pten^{ff}*/Rosa^{tdTomato} and 2 Rosa^{tdTomato} mice 1 year postinjection to illustrate reproducibility in the pattern of retrograde transduction with the parameters used here. Although the injection was done at the L2 vertebral level, the injection sites were centered at the caudal end of the lumbar enlargement; the injection site illustrated in Figure 3A is representative of all other cases (see also Fig. 4*H*). Of note, tdT-labeled CST axons from the lumbar level were brightly fluorescent throughout the rostro-caudal extent of the spinal cord (Fig. 3A–C).

Coronal sections at 0.5-mm interval (Fig. 3D–G) reveal robust labeling of cell bodies and dendrites of CST neurons in layer V, and a light sheet reconstruction from a different mouse reveals the distribution of neurons (Fig. 3*H*). When viewed from above (as in Fig. 3*H*), the dense network of labeled dendrites in layer I/II creates a haze-like cloud over the labeled neuronal cell bodies in layer V, but individual cell bodies become evident with rotation of the 3D image (see Supplementary Movie 0612A). No labeled neurons were seen in the dorsolateral cortex (S2) in mice with L2 injections. Counts using Imaris (Fig. 3*I*) revealed 1394 above threshold hits on the left side and 1517 on the right before editing. After excluding non-neuronal labeling, hits due to labeled dendrites, and scattered hits outside the sensorimotor cortex, there were 1181 labeled CST neurons on the left and 1248 on the right for an average of 1215 labeled CST neurons per side.

Overall, our results indicate that AAV/Cre injections at C5 versus L2 label different populations of neurons, although there may be some overlap in populations in areas posterior to bregma. To determine the extent of overlap of CST neurons labeled by C5 versus L2 injections, we injected retro-AAV/Cre at L2 and retro-AAV/GFP at C5, immunostained brain sections for GFP (FITC), and then imaged sections for GFP immunofluorescence and native tdT fluorescence. For this, it was important to identify a GFP antibody that did not cross-react with the closely related tdT protein. To test for cross-reactivity, sections from mice that received AAV/Cre only were immunostained using 3 commercial GFP antibodies (Invitrogen, rabbit anti-GFP, catalog #A11122; Abcam, goat anti-GFP, catalog #AB6673; and Novus, rabbit anti-GFP, catalog #NB600-308). All GFP antibodies were used at a dilution of 1:1000. As illustrated in Figure 4A–D, there was robust immunostaining of tdT-positive CST neurons when sections were immunostained using GFP antibodies from Abcam and Invitrogen. However, there was no detectable immunofluorescence when sections were immunostained using the GFP antibody from Novus (Fig. 4F). Based on these results, we used the Novus antibody for assessment of double labeling.

The distribution of retrogradely transfected GFP-positive neurons was similar to that reported above with retro-AAV/Cre injections at C5, with large numbers of GFP-positive neurons in the rostral part of the sensorimotor cortex. Similarly, the distribution of tdT-positive neurons labeled by AAV/Cre injections at L2 was similar to the case described above. In the caudal part of the region containing GFP-labeled neurons (~1 mm caudal to bregma), GFP-positive neurons were found in two mediolateral locations separated by a space with few if any GFP-positive neurons (Fig. 4*I*). TdT-positive neurons were detected in the same sections by native fluorescence of tdT (no IHC); these were present in the space between the populations of GFP-positive CST neurons, overlapping the medial area containing GFP-positive neurons (Fig. 4*J*). Although there was overlap in the distribution of GFP- and tdT-positive CST neurons, there were only a few double-labeled neurons. Double-labeled neurons may represent neurons that project to both cervical and lumbar levels or may indicate that injections of AAV/Cre at C5 can lead to transfection of some CST axons passing through cervical levels en route to lower spinal levels. In either case, the number of double-labeled neurons is small.

Although the focus here is on the cells of origin of the CST, cells of origin of other descending pathways to the spinal cord are also labeled following AAV/Cre injections at C5 and L2, including neurons in the red nucleus, reticular formation, vestibular nucleus, and hypothalamus. These can be discerned in the light sheet movies and are evident in cross-sections through the brain (not shown). Of note, with injections at L2, labeled neurons were also seen in Barrington's nucleus, which gives rise to descending pathways that are important for bladder function (not shown).

One other point is that the light sheet images reveal the presence of tdT in the pineal gland (see especially Fig. 4*E*). We reported this phenomenon in abstract form with intracortical injections of AAV (Steward et al. 2016), and a manuscript documenting accumulation of AAV in the pineal gland after injection in different CNS sites is in preparation.

(*C*) Higher magnification view reveals intense tdT fluorescence in nuclei and labeling throughout dendrites including fine dendritic arbors in layers I–II. (*D*) Immunostained section (FITC) illustrating tdT-positive neurons in the main sensorimotor cortex. (*E*) Immunostained section illustrating tdT-positive neurons in the lateral cortex S2. (*F*) Projection image of 3D reconstruction with light sheet microscopy after clearing and immunostaining with iDISCO. Thousands of tdT-positive CMNs are evident in layer V throughout the primary motor, secondary motor, and primary somatosensory cortical areas and S2. IC, internal capsule; Med Pyr, medullary pyramid; Pyr Dec, pyramidal decussation. (*G*) Labeled neurons identified by "Spots" function in Imaris. Numbers of labeled neurons are indicated. Comparison of manual counts of retrogradely labeled CMNS (*H*) with counts from Imaris "Spots" function (*I*). Shaded boxes indicate the 3 counting sites; numbers indicate the counts per site. (*J*) Intact brains and spinal cords from Rosa^{tdTomato} mice 1 year postinjection.

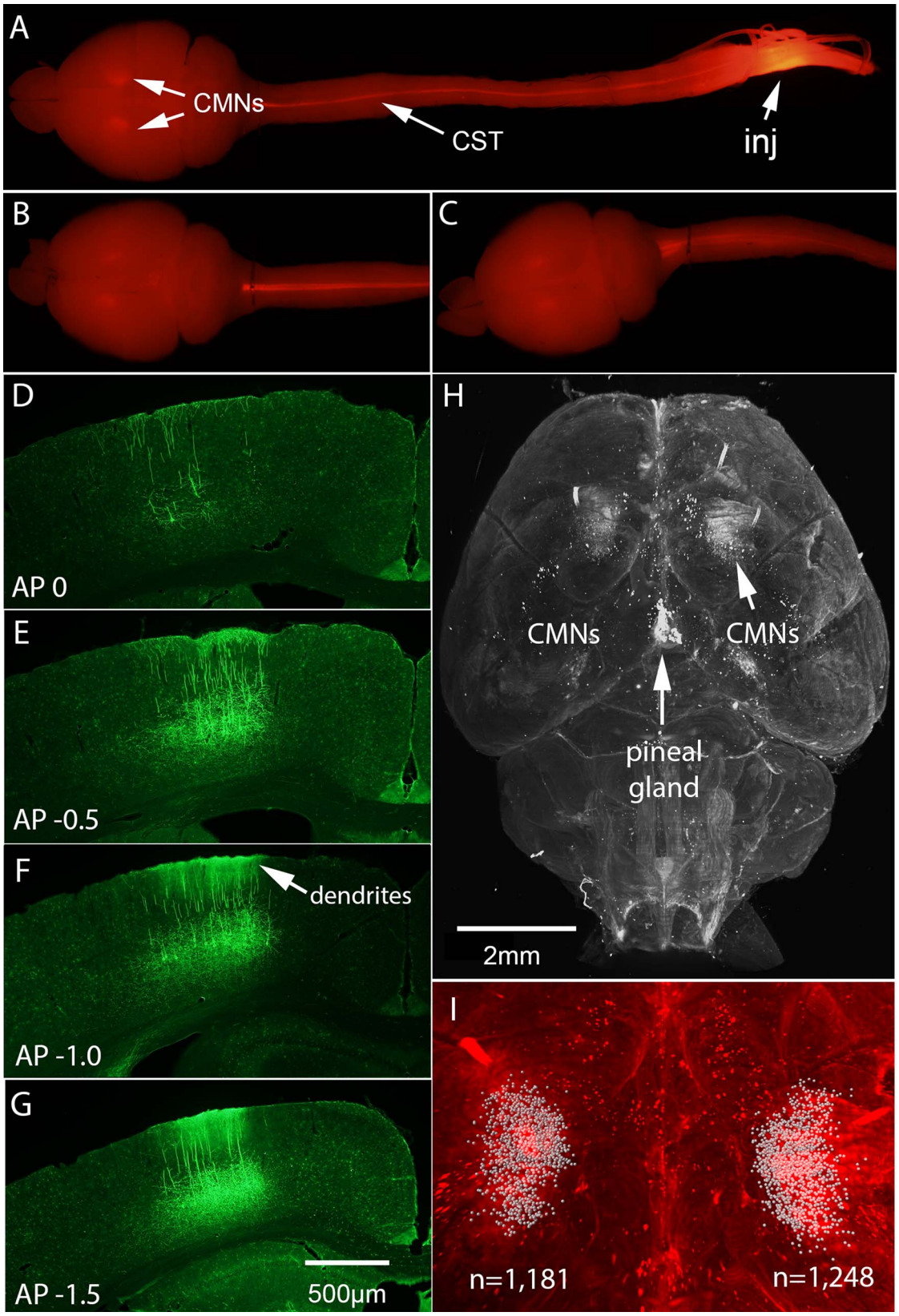

Figure 3. Retrograde transfection of cortical neurons following injections of retrograde-AAV/Cre at L2. (*A–C*) Intact brains and spinal cords from 1 $Pten^{ff}$/$Rosa^{tdTomato}$ and 2 $Rosa^{tdTomato}$ mice 1 year postinjection. (*D–G*) Immunostained sections (FITC) illustrating tdT-positive neurons at different locations with respect to bregma. (*H*) Projection image of 3D reconstruction with light sheet microscopy after clearing and immunostaining with iDISCO. TdT-positive CMNs are present in posterior sensorimotor cortex. (*I*) Labeled neurons identified by "Spots" function in Imaris. Numbers of labeled neurons on each side are indicated. Scale bar in *F* = 500 µm and applies to *D–G*.

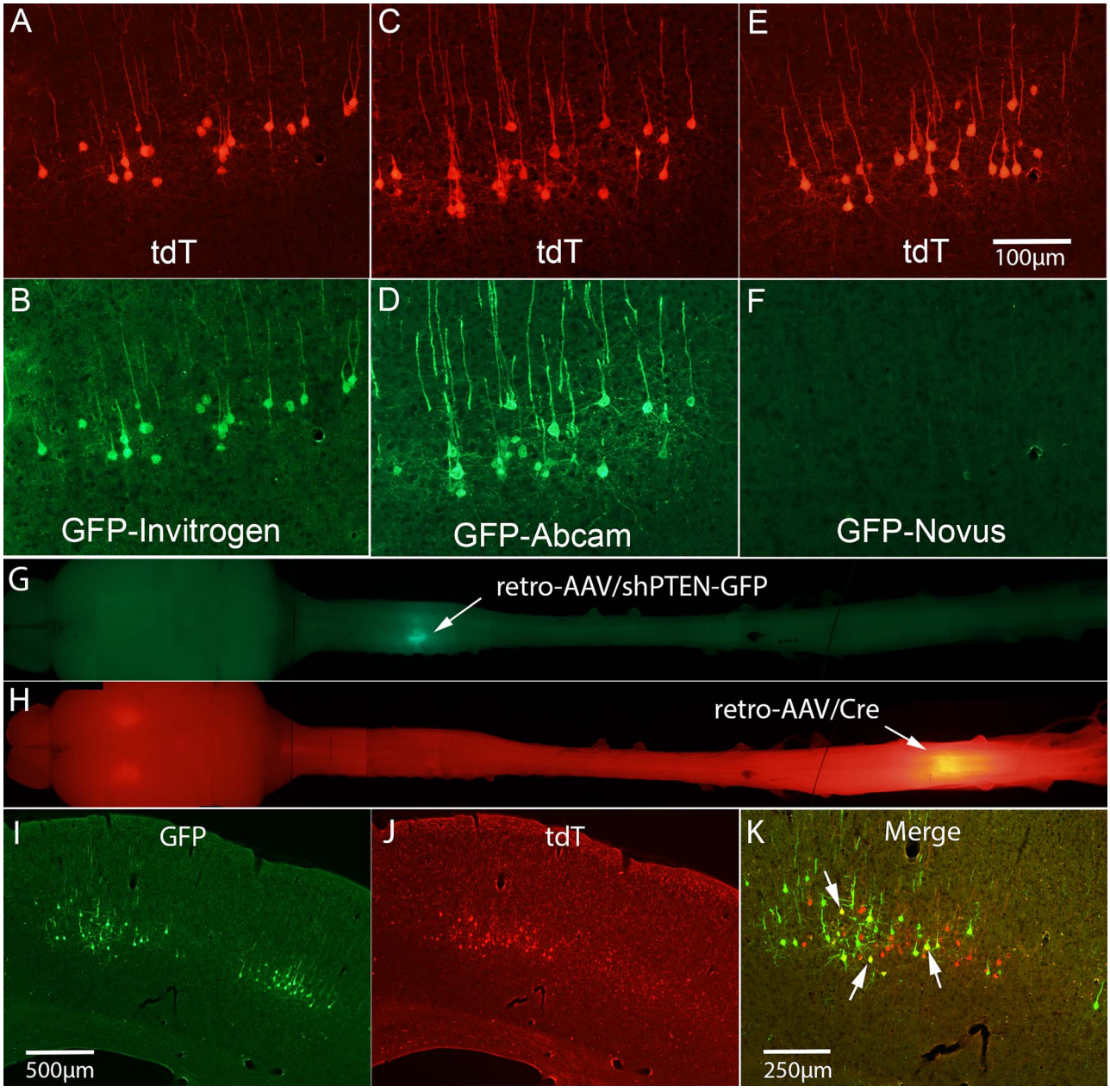

Figure 4. Retrogradely labeled CST neurons with retro-AAV/Cre injections at L2 and retro-AAV/shPTEN-GFP at C5. (*A–E*) Some commercial GFP antibodies recognize tdT. (*A*) Native tdT fluorescence in a section stained for GFP using Invitrogen antibody. (*B*) Immunofluorescence for GFP in same section shown in *A*. (*C*) Native tdT fluorescence in a section stained for GFP using Abcam antibody. (*D*) Immunofluorescence for GFP in same section shown in *C*. (*E*) Native tdT fluorescence in a section stained for GFP using Novus antibody. (*F*) Immunofluorescence for GFP in same section shown in *E*. (*G*) Visualization of GFP fluorescence in intact uncleared brain and spinal cord by fluorescence epi-illumination. (*H*) Visualization of tdT fluorescence in the same brain and spinal cord. (*I*) Coronal section through posterior sensorimotor cortex approximately 1.8 mm caudal to bregma. (*J*) Same section illuminated to reveal native tdT fluorescence. (*K*) Merged image of *I* and *J* to reveal the few double-labeled neurons that were present (arrows). Scale bar in *E* = 100 μm and applies to *A–F*. Scale bar in *I* = 500 μm and applies to *I* and *J*; scale bar in *K* = 250 μm.

BDA Tracing of Corticospinal Projections from Different Cortical Areas

To assess projections from different populations of CMNs, we made single injections of BDA targeting different locations as summarized in Table 1. Actual coordinates of injection sites determined by assessment of coronal sections are mapped in Figure 1*J*; the center of the tracer injection in each mouse is indicated by a colored dot. Different colors indicate injections done on different dates. In what follows, we summarize the distribution of CST axons from representative cases with injections at different rostro-caudal and mediolateral locations.

Dorsomedial Frontal Cortex

In 3 mice, injections were into the most rostral part of the cortex that contains neurons that give rise to the CST based on retrograde labeling studies. Figure 5*A* illustrates a map of the injection sites (0313A-C), in which BDA injections were centered at 2.6–3.0 mm anterior and 0.7–0.8 mm lateral. The injection site

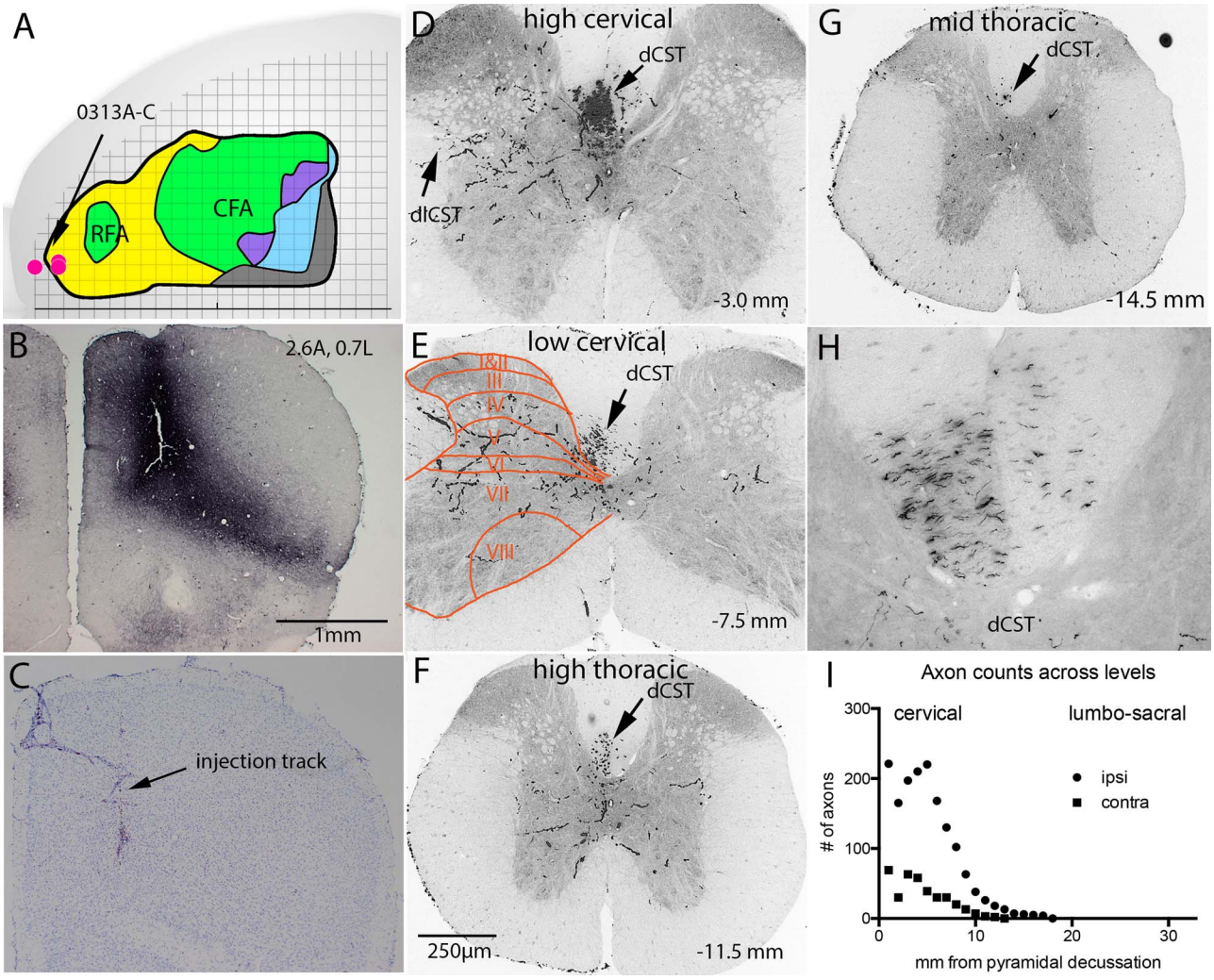

Figure 5. Dorsal frontal cortex projects selectively to cervical and high thoracic levels with terminal arbors in the intermediate lamina and dorsal part of the ventral horn. (*A*) Map of injection sites in which BDA injections were centered at 2.6–3.0 mm anterior and 0.7–0.8 mm lateral. (*B*) Injection site in the case with the largest number of labeled axons (0313C, 2.6 mm anterior, 0.7 mm lateral). (*C*) Cytoarchitecture of the area in a nearby cresyl violet-stained section. (*D–G*) Rostro-caudal distribution of BDA-labeled CST axons. Location of spinal cord laminae is indicated in *E*. Numbers in the lower part of panels *D–G* indicate distance from the pyramidal decussation. (*H*) High magnification view of BDA-labeled axons in the dCST at cervical levels contralateral and ipsilateral to the injection (DAB stain). (*I*) Counts of labeled at 1-mm interval. dCST, dorsal corticospinal tract in the dorsal column; dlCST, dorsolateral corticospinal tract in the dorsal part of the lateral column.

in the case with the largest number of labeled axons (0313C, 2.6 mm anterior, 0.7 mm lateral) is illustrated in Figure 5B, and the cytoarchitecture of the area is illustrated in a nearby cresyl violet stained section in Figure 5C. The rostro-caudal distribution of BDA-labeled CST axons is illustrated in Figure 5D–G. In this and subsequent figures, the distance of each section from the pyramidal decussation is indicated in the lower right of each panel.

To quantify the rostro-caudal extension of BDA-labeled CST axons, we counted labeled axons in the dCST in sections spaced at 1-mm interval. For this, we used sections in which BDA was stained using DAB (Fig. 5H). Counts revealed an average of 203 labeled axons in the dCST in the first 5 sections of the series, 50 labeled axons in the dCST ipsilateral to the cortex of origin, 6 labeled axons in the dlCST, and none in the ventral CST. The number decreased progressively moving from rostral to caudal, so that by mid-thoracic levels (Fig. 5I), only a few labeled axons were present. Of note, the number of BDA axons in the dCST ipsilateral to the injection was relatively high in comparison with most other cases except for the case illustrated in Fig. 8 (more on this below).

Labeled axon arbors were present in the gray matter at cervical through high-thoracic levels and were concentrated in lamina IV–V of the dorsal horn with a few extending into lamina VII of the ventral horn. No labeled axons extended into laminae I–III. The distribution of BDA-labeled arbors across Rexed laminae at low cervical levels is illustrated in Fig. 5E. Terminal arborizations were mainly on the side of the labeled tract, but a few axons also extended across the midline.

Regarding the relatively large number of labeled axons in the dCST ipsilateral to the injection, there did not appear to be spread of BDA to the opposite side. Moreover, although there were hundreds of BDA-labeled CST axons in the medullary pyramid ipsilateral to the injection, careful scanning through sections revealed only 2 BDA-labeled axons in the medullary pyramid contralateral to the injection. Thus, the most likely

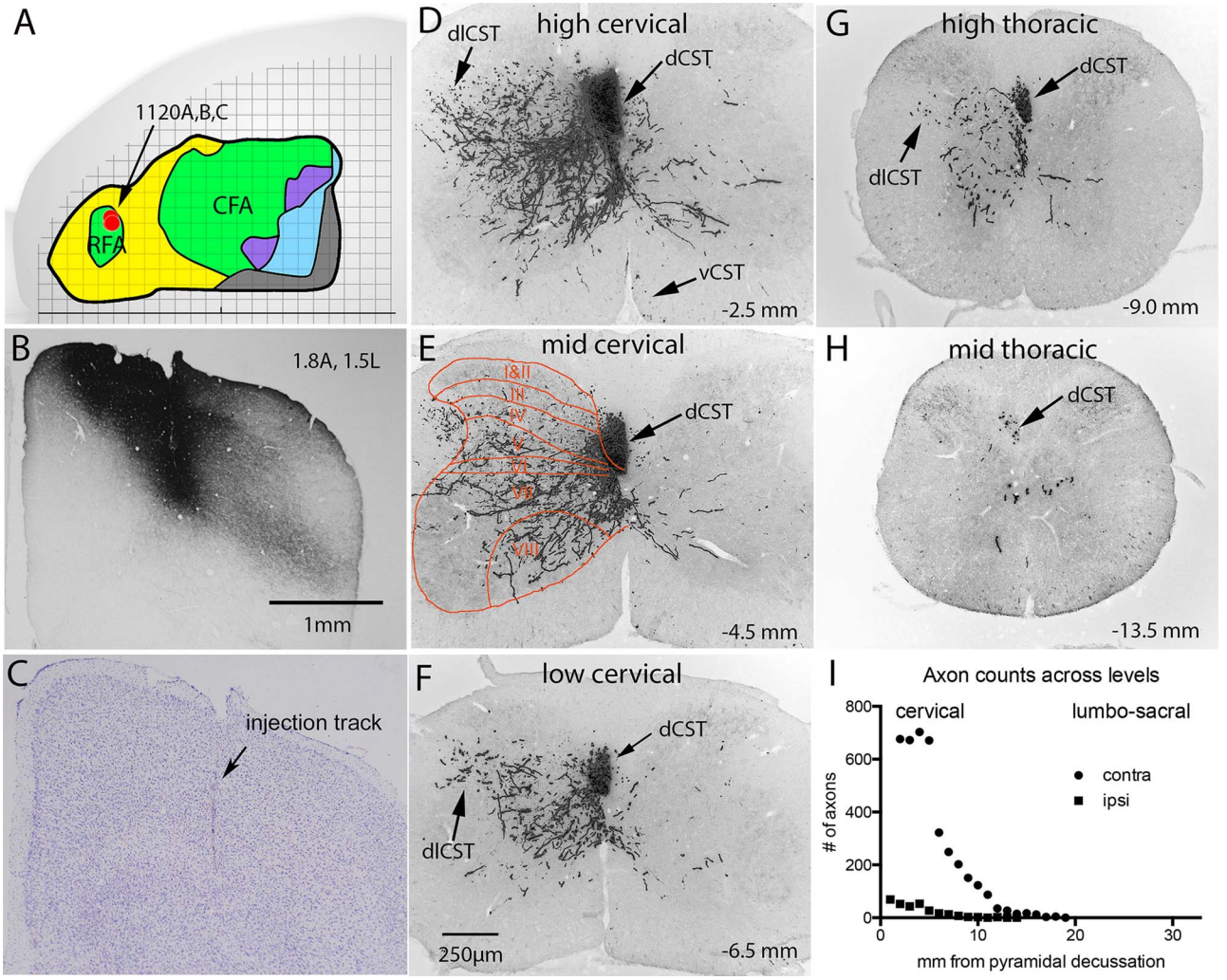

Figure 6. RFA projects selectively to cervical and high thoracic levels with terminal arbors located throughout the intermediate lamina and medial ventral horn. (*A*) Map of injection sites in which BDA injections were centered at 1.8 mm anterior and 1.5–1.6 mm lateral. (*B*) Injection site in the case with the largest number of labeled axons (1120C). (*C*) Cytoarchitecture of the area in a nearby cresyl violet-stained section. (*D–H*) Rostro-caudal distribution of BDA-labeled axons. Location of spinal cord laminae is indicated in *E*. Numbers in the lower part of panels *D–H* indicate distance from the pyramidal decussation. (*I*) Counts of labeled axons at 1-mm interval. vCST, labeled axons in the ventral column ipsilateral to the cortex of origin in the expected location of the ventral CST. Other abbreviations are as in Figure 5.

explanation for the relatively large number of BDA-labeled axons in the dCST ipsilateral to the injection is that these axons failed to cross at the pyramidal decussation.

Rostral Forelimb Area

In 3 mice, injections were into the rostral part of the sensorimotor cortex that was identified as the rostral forelimb area (RFA) in microstimulation studies (Tennant et al., 2010). Figure 6A illustrates a map of the injection sites (1120A-C), in which BDA injections were centered at 1.8 mm anterior and 1.5–1.6 mm lateral (medial part of the forelimb cortex; M1). The injection site in the case with the largest number of labeled axons (1120C) is illustrated in Figure 6B, and the cytoarchitecture of the area is illustrated in a nearby cresyl violet-stained section in Figure 6C. The rostro-caudal distribution of CST axons is illustrated in Figure 6D–H. The number of BDA-labeled axons in all tracts decreased rapidly moving from rostral to caudal; few labeled axons extended to the mid-thoracic level (Fig. 6H) and none extended to lower thoracic levels.

Counts of labeled CST axons in the dCST (Fig. 6I) revealed over 1000 in the first section of the series (not shown on graph) and then an average of 680 in the next 4 sections. The number of labeled axons decreased progressively moving caudally, and no labeled axons extended further than mid-thoracic levels. In addition to the main tract in the dCST, there were 65 labeled axons in the dlCST at mid cervical levels (Fig. 6E) and an average of 54 labeled axons in the dCST ipsilateral to the injection. In this case, there were also 7 BDA-labeled axons in the ventral column contralateral to the main labeled tract in the position expected for the vCST (arrow, Fig. 6D). Labeled axons in the vCST were present in only a minority of mice as noted below.

At cervical levels, labeled axons extended from the dCST and dlCST into the gray matter, where they gave rise to dense terminal arbors in laminae IV–VIII, except for the lateral part of lamina VII (Fig. 6D–F). The distribution of BDA-labeled arbors across Rexed laminae at mid cervical levels is illustrated in Figure 6E. Only a few labeled arbors extended into the lateral part of the ventral horn or into laminae I–III. A moderate number

of axons extended across the midline to arborize in the gray matter of the medial ventral horn on the contralateral side (Fig. 6A–D). The density of the arbors decreased moving caudally in parallel with the number of axons in the dCST.

Medial Anterior Forelimb Cortex

In 4 mice, injections were clustered at 0.6–1.0 mm anterior and 0.7–1.1 mm lateral (Fig. 7A); in these cases, most axons terminated at cervical levels but some extended through thoracic and a few axons extended to high lumbar levels. The injection site in the case with the largest number of labeled axons is illustrated in Figure 7B, and the cytoarchitecture of the area is illustrated in a nearby cresyl violet-stained section in Figure 7C. The rostro-caudal distribution of CST axons is illustrated in Figure 7D–H and counts of BDA-labeled axons in the dCST are illustrated in Figure 7I. At cervical levels, counts ranged from 248 to 349 (average of 255 in the first 9 sections of the series), with 10 labeled axons in the dCST contralateral to the main labeled tract and no labeled axons in the ventral CST. About 10% of the labeled axons extended in the dCST into thoracic levels and a few extended into high lumbar segments (Fig. 7H; insets illustrate labeled axons in the dCST and labeled arbors in gray matter).

At cervical levels, the distribution of labeled terminal arbors was similar to that in Figure 6. Labeled axons extended from the dCST and dlCST into laminae IV–VIII, except for the lateral part of layer VII (Fig. 7D,E), with a few axons extending to the ventromedial boundary of the ventral horn (Fig. 7E). Only a few labeled arbors extended into the lateral part of the ventral horn or into laminae I–III. At mid-thoracic levels, axons could be seen streaming from the dCST into the medial–dorsal part of lamina VII. In contrast to the case illustrated in Figure 6, there were very few recrossing axons.

Medial Posterior Forelimb Cortex

In 3 mice, injections were into the medial part of the posterior forelimb cortex; actual coordinates were 0, 0.2, and 0.4 mm anterior and 1.0, 1.1, and 1.2 mm lateral (See Fig. 8A for a map of injection sites). In the case with the fewest labeled axons (about 80 BDA-labeled axons in the dorsal CST at high cervical levels), projections were to the cervical region only as in the cases injected at 0.5–1.0 anterior. In the 2 other cases, labeled axons extended to lumbar and sacral levels. The injection site in the case with the largest number of labeled axons (1120E) is illustrated in Figure 8B, the cytoarchitecture of the area is illustrated in a nearby cresyl violet-stained section in Figure 8C, the rostro-caudal distribution of CST axons is illustrated in Figure 8D–H, and the counts of BDA-labeled axons in the dCST are illustrated in Figure 8I. At high cervical levels, there were over 700 labeled axons in the dCST contralateral to the injection (average of 711 across 5 sections), 50 labeled axons in the dCST ipsilateral to the injection, 40 labeled axons in the dlCST, and 2 labeled axons in the vCST. Labeled axons in the dlCST are especially evident at thoracic levels (Fig. 8F). There were also 8 labeled axons in the lateral column contralateral to the main labeled tract (arrows with asterisk in Figure 8C); this is an unusual location for CST axons but has been previously been reported in mice (Zheng et al. 2006) and rats (Brosamle and Schwab 1997).

In contrast to Figures 5–7, labeled axon arbors in the gray matter were dense at all rostro-caudal levels. However, the distribution across laminae was similar to that in Figures 5–7. At cervical levels, dense axon arbors were present in laminae IV–VIII, except for the lateral part of layer VII (Fig. 8D,E). Some axons extended to the ventromedial boundary of the ventral horn (Fig. 8E), but only a few extended into the lateral part of the ventral horn or into laminae I–III. At thoracic levels, the highest density of labeled arbors was in the medial part of laminae V–VII (Fig. 8F); of note, labeled axons could be seen streaming from the dlCST toward the dense arbors in lamina V (Fig. 8F, unlabeled arrow). At lumbar and sacral levels, labeled arbors were dense in laminae IV–V and the medial part of laminae VII–VIII (Fig. 8G,H). At all levels, a moderate number of labeled axons recrossed the midline to arborize on the side contralateral to the labeled tract.

Anterior-Lateral Forelimb Cortex

In 3 mice, injections were into the anterior-lateral part of the forelimb cortex (coordinates were 0.7–1.0 mm anterior and 2.2–2.3 mm lateral (See Fig. 9A for a map of injection sites). In these cases, labeled axons were also restricted primarily to cervical levels, but the distribution of labeled terminal arbors in the gray matter of the spinal cord was different than in cases with injections into medial forelimb regions.

Figure 9 illustrates the case with the largest number of labeled axons (0812D) in which the BDA injection was centered 1 mm anterior and 2.3 mm lateral (lateral M1/S1 border). The injection site is illustrated in Figure 9B, the cytoarchitecture of the area is illustrated in a nearby cresyl violet-stained section in Figure 9C, the rostro-caudal distribution of CST axons is illustrated in Figure 9D–H, and the counts of BDA-labeled axons in the dCST are illustrated in Figure 9I. At high cervical levels, counts revealed an average of 510 labeled axons in the dCST contralateral to the injection in the first 6 sections of the series and 10 labeled axons in the dlCST. Of note, there were also a large number of labeled axons in the dCST ipsilateral to the injection (average of 199 in the first 6 sections of the series). The number of labeled axons in the dCST decreased moving from cervical to thoracic levels, and very few axons extended to lumbar levels (5 labeled axons are present at the level indicated in Fig. 9H).

In contrast to what was seen with injections into the medial forelimb cortex, BDA-labeled arbors were most dense in the medial part of laminae III–VI, and fewer axons extended into laminae VII–VIII (Fig. 9E). There were a moderate number of labeled axon arbors in laminae III–V on the contralateral side. The density of the labeled arbors decreased moving caudally in parallel with the decrease in numbers of BDA-labeled axons in the dCST. Despite the low number of labeled axons that extended to lumbar levels, there were occasional labeled arbors in the gray matter (Fig. 9H illustrates an arbor on the side ipsilateral to the cortex of origin).

Two technical points regarding the case illustrated in Figure 9 deserve further consideration. First, intense BDA staining extends well beyond the injection track, especially laterally. Importantly, the distribution of labeled CST axons was similar in the two other cases with injections at the same site where the BDA labeling appeared more focal. The second point pertains to the relatively large number of labeled axons in the dCST ipsilateral to the injection. As in the case illustrated in Figure 5, there were hundreds of BDA-labeled CST axons in the medullary pyramid ipsilateral to the injection, but there was only one BDA-labeled axon in the medullary pyramid contralateral to the injection. This further supports the interpretation that BDA-labeled axons in the dCST ipsilateral to the injection failed to cross at the pyramidal decussation.

Posterior-Lateral Forelimb Cortex

In 4 mice, injections were in the posterior-lateral forelimb cortex (0.2–0.8 mm posterior, 1.8–2.3 lateral, see Fig. 10A for a map

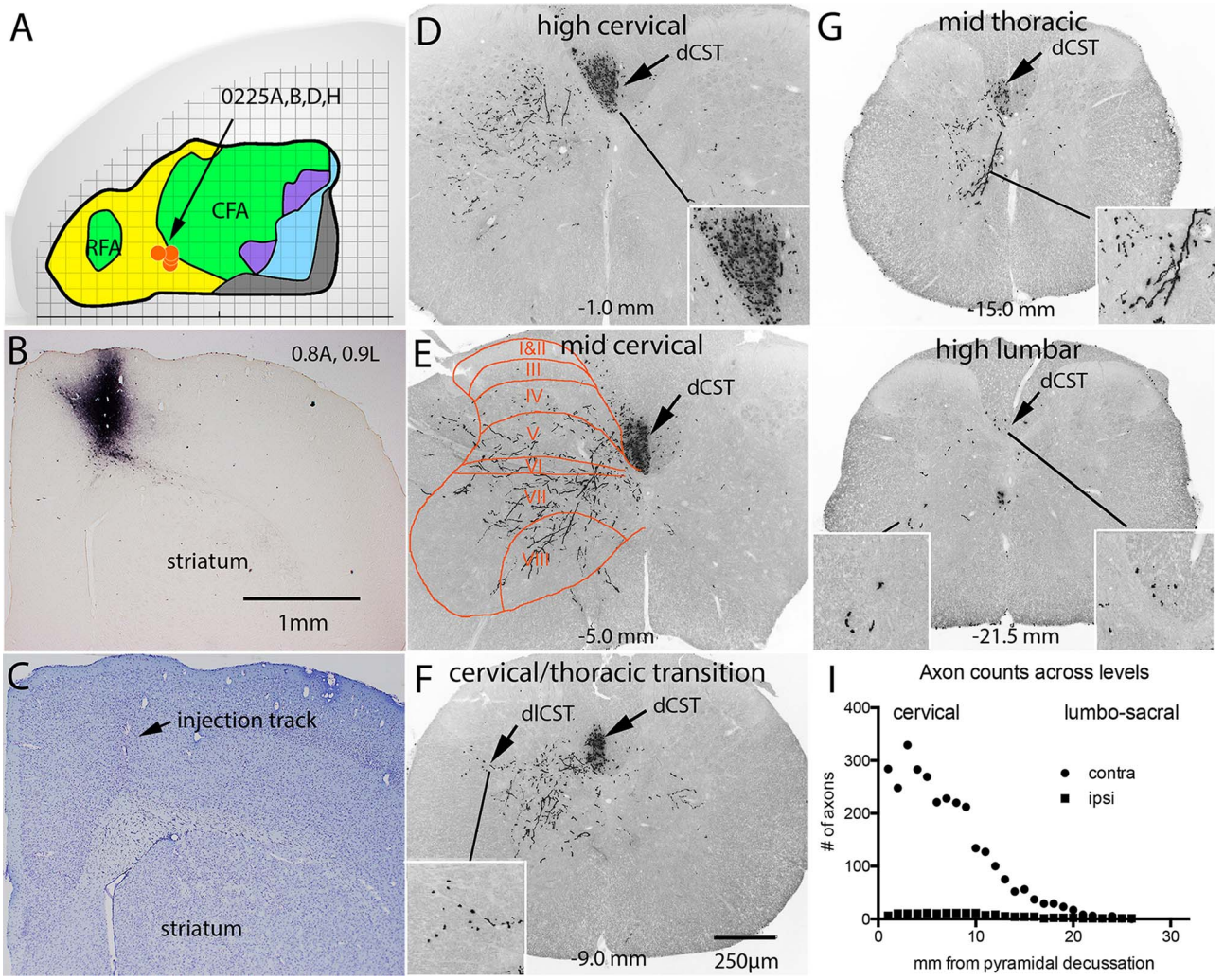

Figure 7. Medial anterior forelimb cortex projects selectively to cervical and mid-thoracic levels with terminal arbors located throughout the intermediate lamina and medial ventral horn. (*A*) Map of injection sites at 0.6–0.8 mm anterior, 0.9–1.1mm lateral. (*B*) BDA labeling at injection site. (*C*) Cresyl violet-stained section at injection site. (*D–H*) Cy3-labeled axons at cervical-high lumbar levels following a single injection of BDA at 0.8 anterior and 0.9–1.1 mm lateral. Location of spinal cord laminae is indicated in *E*. Insets show axons in the dlCST and dCST at ×2 higher magnification. Numbers in the lower part of panels *D–H* indicate distance from the pyramidal decussation (*I*) Counts of labeled axons in the dCST in sections spaced at 1-mm interval. Abbreviations are as in Figure 5.

of injection sites). Figure 10*B* illustrates the injection site in the case with the largest number of labeled axons (0812D) in which the BDA injection was centered 0.8 mm posterior and 2.4 mm lateral. The cytoarchitecture of the area is illustrated in a nearby cresyl violet-stained section in Figure 10*C*, the rostro-caudal distribution of CST axons is illustrated in Figure 10*D–H*, and counts of BDA-labeled axons in the dCST are illustrated in Figure 10*I*.

In all cases, there were several hundred BDA-labeled axons in the dorsal CST at high cervical levels (average of 360 labeled axons in the first 9 sections of the series in Fig. 10*F*). There were a relatively low number of labeled axons (less than 5) in the dCST contralateral to the main labeled tract and a moderate number of labeled axons (15–50) in the dlCST at cervical levels. One of the 4 mice had about 6 labeled axons in the vCST contralateral to the main labeled tract; the other 3 mice had none. The number of labeled axons in the dCST remained high through mid-thoracic levels (Fig. 10*F*), dropping off at lumbar levels (Fig. 10*G*). Only a few labeled axons continued to low lumbar levels (Fig. 10*H*, inset).

In 3 cases, labeled arbors were most dense in the medial part of laminae III-V with a sharp boundary at layer II/III. In the case with an injection centered at 0.4 posterior and 2.0 lateral, labeled axon arbors were most dense in more lateral portions of laminae 3–5 (not shown). In all cases, very few axons extended into the ventral horn. The distribution of labeled axons was very similar in an additional case with an injection centered at 1.5 mm posterior, 2.0 lateral (0812H in Fig. 10*A*). A noteworthy feature with injections in the posterior-lateral forelimb region site was the relative lack of recrossing projections; there were elaborate arbors ipsilateral to the main labeled tract but very few axons extended across the midline to the side contralateral main labeled tract.

Caudal Sensorimotor Cortex

In 4 mice, injections were into the medial hindlimb cortex at 0.9–1.3 mm posterior to bregma, 1.0–1.5 mm lateral (see Fig. 11*A* for a map of injection sites). In all these cases, BDA-labeled axons extended through cervical levels without sending extensive

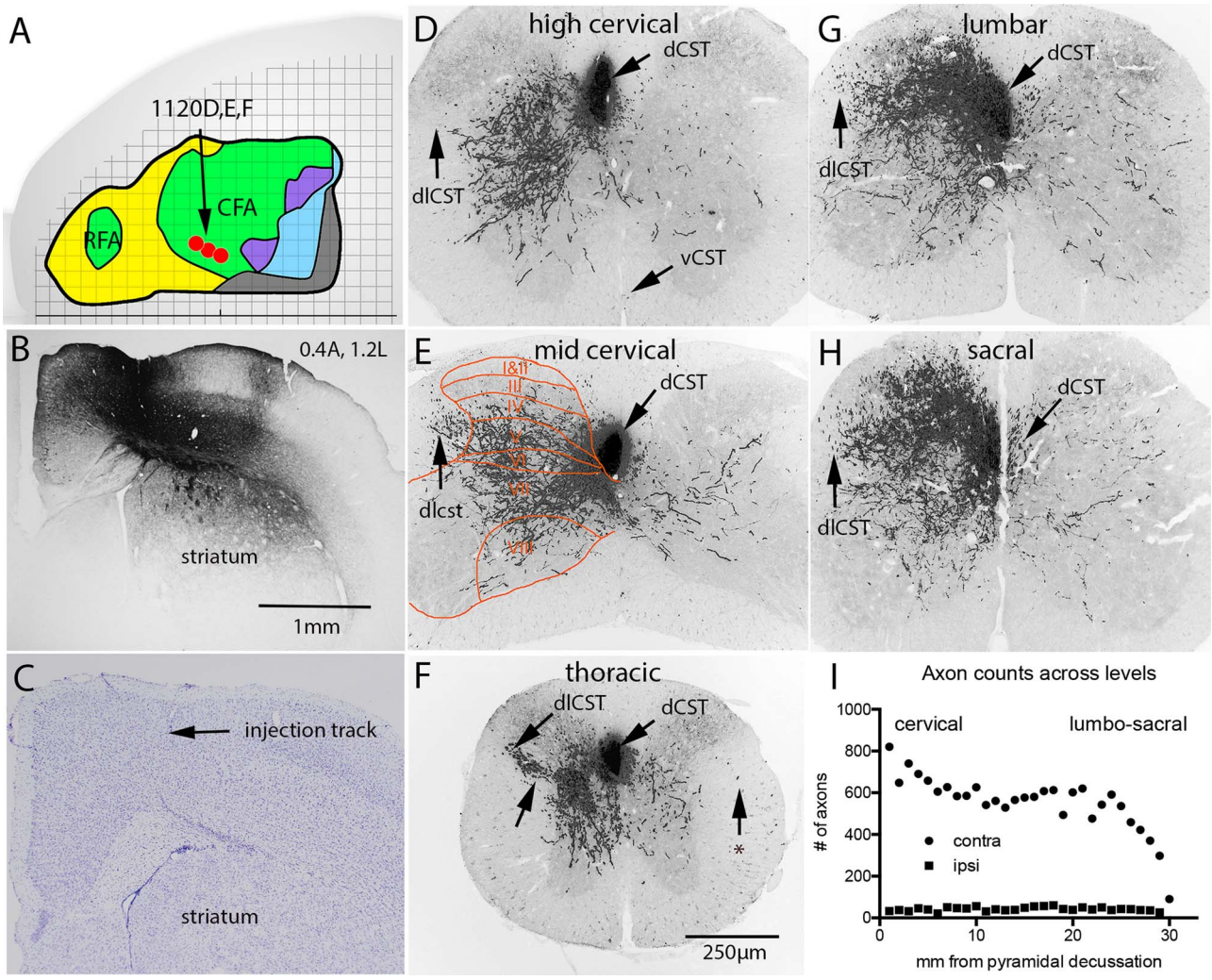

Figure 8. Medial posterior forelimb cortex projects to cervical–sacral levels with terminal arbors throughout the intermediate lamina and medial ventral horn. (*A*) Map of injection sites at 0, 0.2, and 0.4 mm anterior and 1.0, 1.1, and 1.2 mm lateral. (*B*) BDA labeling at injection site. (*C*) Cresyl violet-stained section at injection site. (*D–H*) Cy3-labeled axons at cervical–sacral levels following a single injection of BDA at 0.4 mm anterior and 1.2 mm lateral. Location of spinal cord laminae is indicated in *E*. Numbers in the lower part of panels *D–H* indicate distance from the pyramidal decussation. (*I*) Counts of labeled axons in the dCST in sections spaced at 1-mm interval. Abbreviations are as in Figure 5. Asterisk in *F* indicates a few labeled axons in the lateral column ipsilateral to the injected cortex.

collaterals into the gray matter and then arborized extensively at lumbar–sacral levels. Figure 11 illustrates the case (1120I) with the most extensive labeling in which the BDA injection was centered 0.9 mm posterior and 1.1 mm lateral. The injection site is illustrated in Figure 11*B*, the cytoarchitecture of the area is illustrated in a nearby cresyl violet-stained section in Figure 11*C*, the rostro-caudal distribution of CST axons is illustrated in Figure 11*D–H*, and counts of BDA-labeled axons in the dCST are illustrated in Figure 11*I*.

Throughout cervical levels (first 10 sections of the series), counts revealed an average of 717 labeled axons in the dCST contralateral to the injection, with 25 labeled axons in the dCST contralateral to the cortex of origin and 35 in the dlCST (Fig. 11*D–F*; insets show high magnification views of the dlCST). There were no labeled axons in the ventral column ipsilateral to the injection in the position of the vCST. The number of labeled axons in the dCST remained high (average of 704) throughout thoracic and lumbar levels, and 178 axons extend to sacral levels (graph in Fig. 11*I*).

There were very few BDA-labeled arbors in the gray matter at cervical levels (Fig. 11*D,E*) with increasing numbers of arbors in the gray matter moving caudally (Fig. 11*E,F*), reaching maximal density at lumbar levels (Fig. 11*G*). At thoracic levels, arbor density was highest in laminae III–VI of the dorsal horn and a few axons extended into lamina VII in the ventral horn (Fig. 11*E*). At lumbar levels, very elaborate axon arbors extended throughout laminae III–V of the dorsal horn, and a few axons extended into the medial part of lamina VII in the ventral horn. Some labeled axons extended across the midline at lumbar levels, and there were large numbers of recrossing axons in sacral segments (Fig. 11*H*).

In 4 mice, injections were into the medial sensorimotor cortex at 1.5–2 mm posterior to bregma (about 1.0 mm further posterior than the cases illustrated in Fig. 11) and 1.2–1.6 mm lateral (see Fig. 12*A* for a map of injection sites). This is into a part of the sensorimotor cortex that has been identified as activating the trunk and tail in previous mapping studies (Tennant et al., 2010). In these cases, BDA-labeled axons extended through cervical

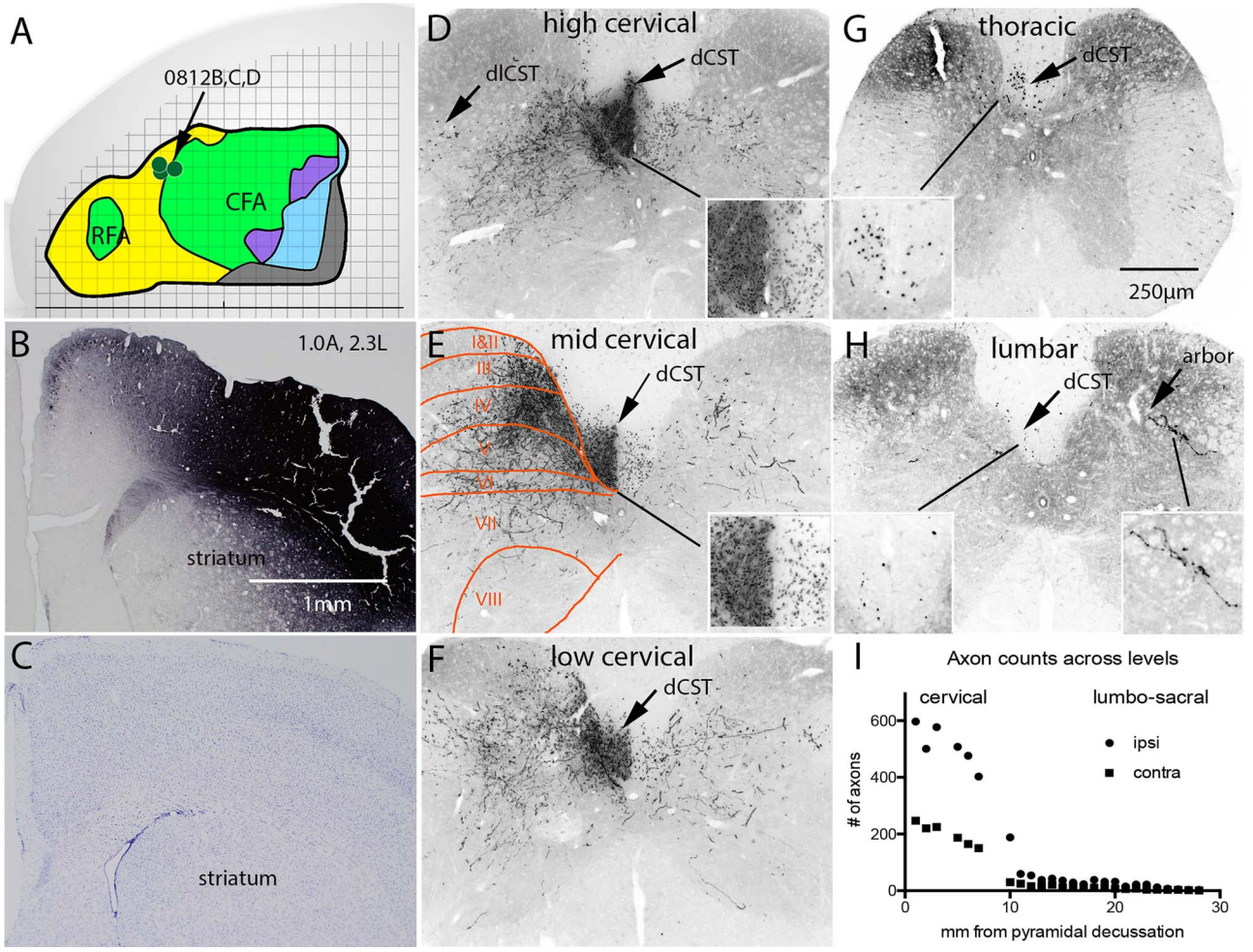

Figure 9. Anterior-lateral forelimb cortex projects selectively to cervical levels with terminal arbors in the dorsal intermediate lamina and medial ventral horn. (*A*) Map of injection sites 0.7–1.0 mm anterior and 2.2–2.3 mm lateral. (*B*) BDA labeling at injection site in the case with the most labeled axons. (*C*) Cresyl violet-stained section at injection site. (*D–H*) Cy3-labeled axons at different levels following a single injection of BDA at 1.0 mm anterior and 2.3 mm lateral. Note large number of labeled axons in the dCST ipsilateral to the cortex of origin (insets in *A* and *B*) and that, although very few axons extend to lumbar levels, there are occasional arbors in the gray matter (*H*, arbor). Location of spinal cord laminae is indicated in *E*. Insets show axons in the dlCST and dCST at ×2 higher magnification. Numbers in the lower part of panels *D–H* indicate distance from the pyramidal decussation. (*I*) Counts of labeled axons in the dCST in sections spaced at 1-mm interval. Abbreviations are as in Figure 5.

levels with essentially no collaterals into the cervical gray matter and then arborized extensively at lumbar–sacral levels. Figure 12 illustrates the case (0321H) with the most extensive labeling in which the BDA injection was centered 2.0 mm posterior and 1.5 mm lateral. The injection site is illustrated in Figure 12*B*, the cytoarchitecture of the area is illustrated in a nearby cresyl violet-stained section in Figure 12*C*, the rostro-caudal distribution of CST axons is illustrated in Figure 12*D–H*, and counts of BDA-labeled axons in the dCST are illustrated in Figure 12*I*.

Throughout cervical levels, counts revealed an average of 347 labeled axons in the dCST contralateral to the injection (graph in Fig. 12*I*), with 6 labeled axons in the dCST contralateral to the cortex of origin and 8 in the dlCST. There were no labeled axons in the ventral column ipsilateral to the injection in the position of the vCST. The number of labeled axons in the dCST remained around 300 through thoracic and lumbar levels and then fell off at sacral levels.

The distribution of labeled arbors across spinal cord laminae was more limited than in the case illustrated in Figure 11. Elaborate axon arbors extended throughout laminae III–V of the dorsal horn in lumbar and sacral segments (Fig. 12*G,H*), but very few axons extended into the medial part of lamina VII in the ventral horn, and there were only a few recrossing axons in sacral segments (Fig. 12*H*).

In one additional mouse, the injection was centered in a more lateral location in the most posterior sensorimotor cortex (1.8 mm posterior to bregma, 2.0 mm lateral). In this case, the distribution of axon arbors across spinal laminae was very similar to that of case illustrated in Figure 12. Specifically, axon arbors were restricted largely to laminae III–V of the dorsal horn and did not extend into the ventral horn.

Dorsolateral Cortex (S2)

Three mice (0408A-C) received injections targeting CST neurons in the dorsolateral cortex. Target coordinates were 1.0 mm posterior and 3.2 mm lateral and 1.1 mm deep, and actual coordinates were 1.0, 1.8, and 2.0 mm posterior and 3.4, 3.5, and 3.6 mm lateral. The distribution of labeled axons in the spinal cord was similar in all 3 cases, and the case with the largest number of

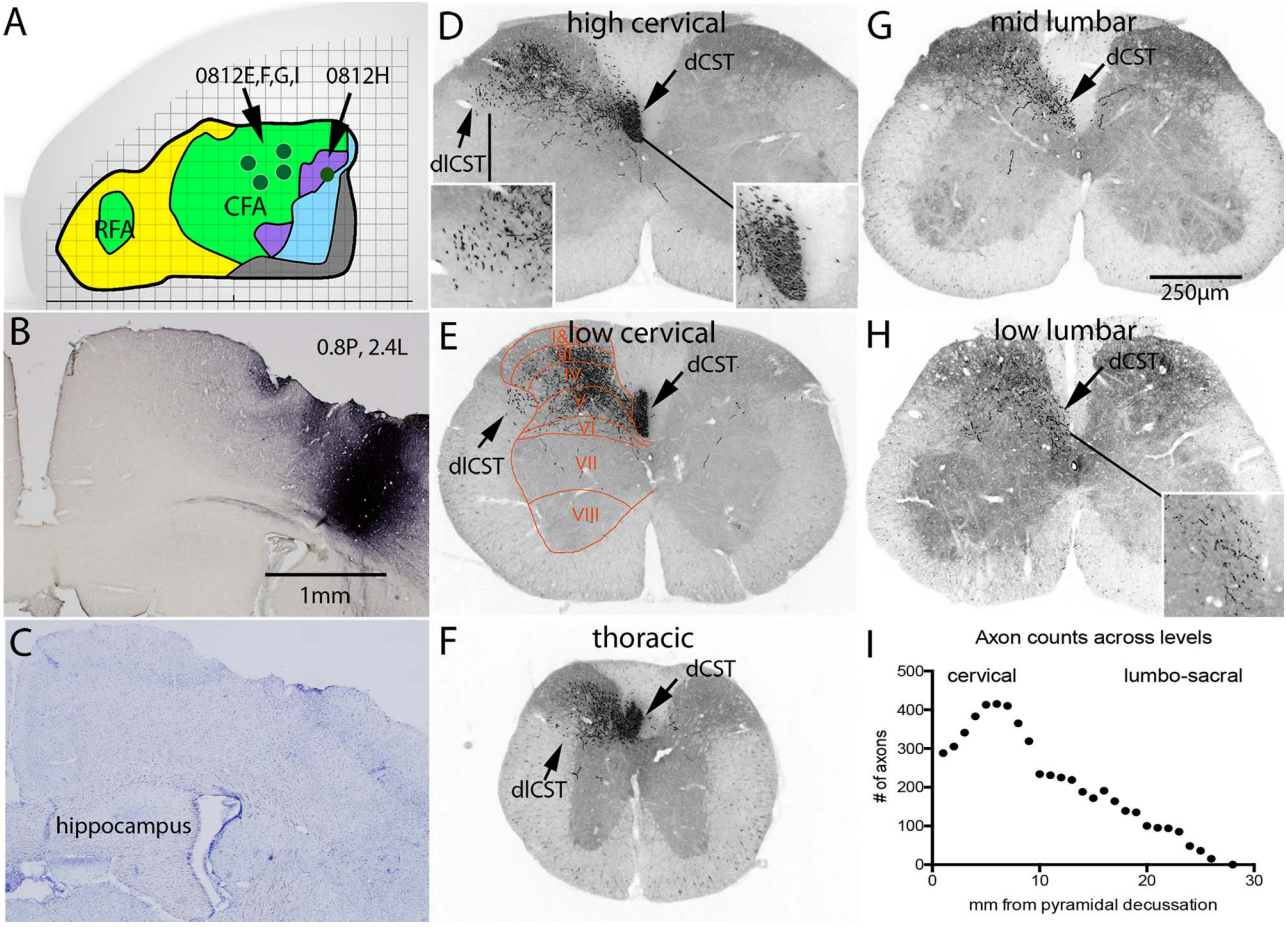

Figure 10. Posterior-lateral sensorimotor cortex projects to cervical–lumbar levels with terminal arbors in the medial portion of the dorsal horn. (*A*) Map of injection sites. (*B*) BDA labeling at injection site in the case with the most labeled axons. (*C*) Cresyl violet-stained section at injection site. (*D–H*) Cy3-labeled axons at different levels following a single injection of BDA at 0.8 mm posterior and 2.4 mm lateral. Location of spinal cord laminae is indicated in *E*. Insets show axons in the dlCST and dCST at ×2 higher magnification. Numbers in the lower part of panels *D–H* indicate distance from the pyramidal decussation. (*I*) Counts of labeled axons in the dCST in sections spaced at 1-mm interval. Insets show high magnification views of labeled axons. Abbreviations are as in Figure 5.

labeled axons is illustrated in Figure 13. At high cervical levels, counts revealed 396 and 347 labeled axons in the dlCST in the first 2 sections of the series, with 8 axons in the dlCST and none in the ventral column. The number of labeled axons decreased progressively through the cervical levels and no labeled axons extended beyond low cervical levels.

Axon arbors were concentrated in the medial part of lamina 5 of the dorsal horn just lateral to the dorsal column. A few labeled axons extended dorsally into the dorsal horn, and a very few extended into the ventral horn. There was a prominent field of labeled axons rostral to the pyramidal decussation in spinal trigeminal "nucleus caudalis" (not shown).

Notes on Laterality

In rats, the majority of CST axons from all cortical locations descend in the dorsal column (dorsal CST) contralateral to the cortex of origin, with smaller numbers of axons in the dorsolateral CST in the lateral column and the ventral CST in the ventral column. The dCST and dlCST are crossed, whereas the vCST is ipsilateral to the cortex of origin. As in our previous studies (Zheng et al. 2003; Steward et al. 2004, 2008), most mice did not have labeled axons in the ventral column ipsilateral to the cortex of origin in the location of the ventral CST. However, in all mice, there were a few labeled axons in the dCST ipsilateral to the cortex of origin, and some mice had relatively large numbers of such axons (Figs 5 and 9). This variability in the number of ipsilateral dCST axons did not appear to be systematic, for example, related to location in the cortex, so we attribute this to biological variability. The other aspect of laterality pertains to axons that recross at spinal levels to terminate on the side ipsilateral to the cortex of origin. In general, the number of recrossing axons also varied across cases in a way that did not appear to be systematic, except that recrossing axons were most common at sacral levels (Figure 11).

Discussion

Our assessment of the degree to which different parts of the sensorimotor cortex in mice project selectively to different rostrocaudal levels of the spinal cord yielded several conclusions, summarized in Figure 14: 1) CST axons from the rostral part of the sensorimotor cortex, including the RFA, terminate primarily at cervical levels and did not extend beyond mid-thoracic levels; 2) CST axons from the posterior sensorimotor cortex (hindlimb/trunk region) pass through cervical regions without extending

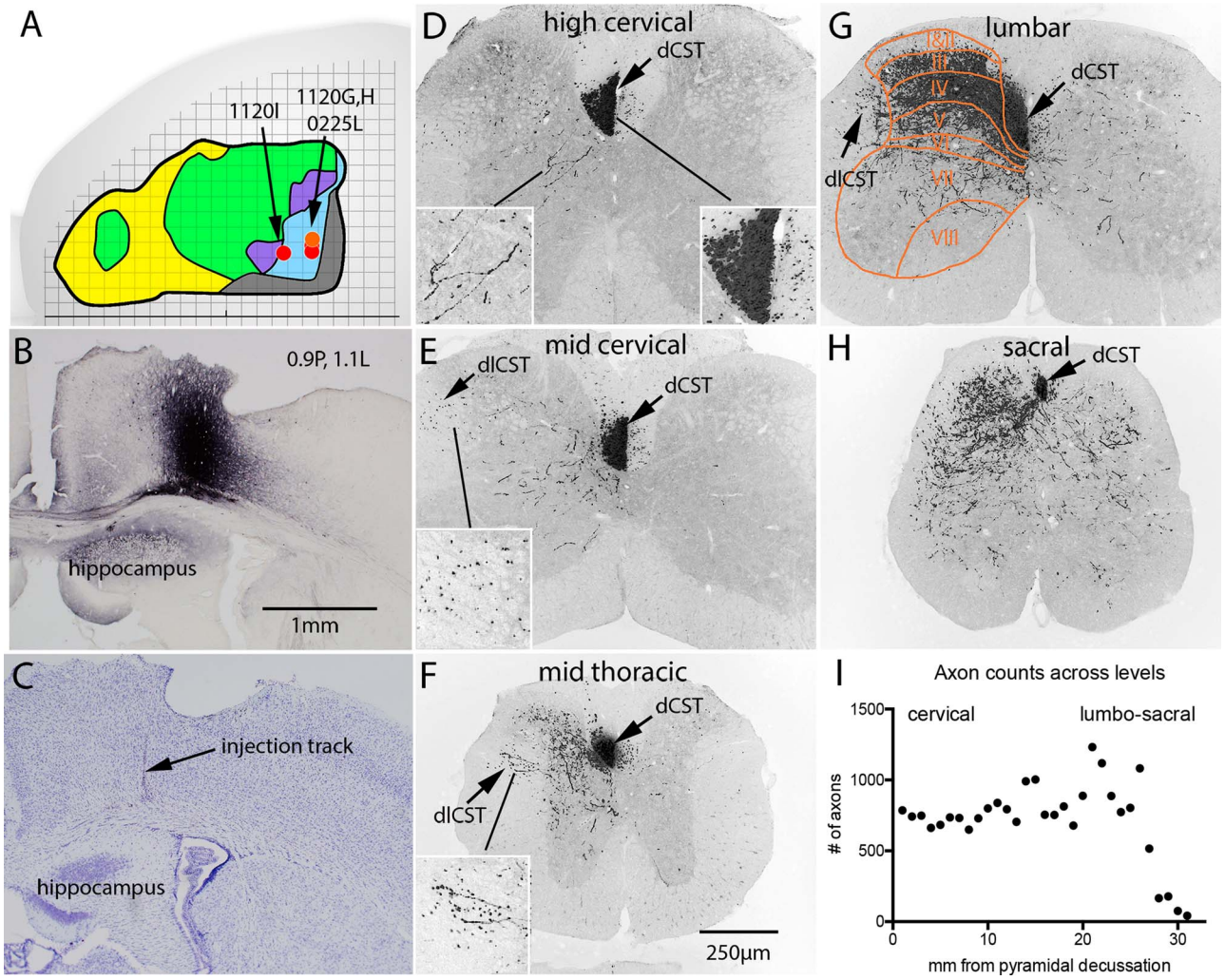

Figure 11. Posterior-medial sensorimotor cortex (hindlimb region) projects to cervical–sacral levels with terminal arbors located primarily in the dorsal horn. (*A*) Map of injection sites. (*B*) BDA labeling at injection site in the case with the most labeled axons. (*C*) Cresyl violet-stained section at injection site. (*D–H*) Cy3-labeled axons at different levels following a single injection of BDA at 0.9 mm posterior and 1.1 mm lateral. Insets show axons in the dlCST and dCST at ×2 higher magnification. Location of spinal cord laminae is indicated in *G*. Numbers in the lower part of panels *D–H* indicate distance from the pyramidal decussation. (*I*) Counts of labeled axons in the dCST in sections spaced at 1-mm interval. Insets show high magnification views of labeled axons. Abbreviations are as in Figure 5.

collaterals into the gray matter and then arborize extensively in the gray matter in lumbar–sacral segments; 3) the caudal forelimb area (CFA) between these two innervates cervical through sacral levels; 4) CST axons from the dorsolateral cortex near the barrel field project exclusively to the high cervical level, arborizing in a small region adjacent to the dorsal column; 5) the degree of bilaterality of CST terminal arbors varies by spinal level, with the most extensive bilateral projections being at sacral levels; 6) one of the descending pathways seen in other species including rats (the ventral CST) is very sparse in the strains of mice that we studied; 7) consistent with previous studies in rats (Bareyre et al. 2002), CST axons from the rostro-medial sensorimotor cortex terminate primarily in intermediate laminae in the spinal cord with some arbors extending into the ventral horn, whereas CST axons from the rostro-lateral and posterior sensorimotor cortex terminate primarily in the dorsal horn. In what follows, we discuss these points along with technical considerations and caveats.

Distribution of the Cells of Origin of the CST in Mice

The overall distribution of retrogradely labeled neurons following retro-AAV/Cre or fluorogold injections at C5 is similar to what we and others have previously described in rats (Nielson et al. 2010, 2011; Liang et al. 2011). Our results are also in agreement with the retrograde mapping studies of Wang et al. (2018) that used retro-AAV encoding fluorescent protein reporters and recent reports using fluorescent microspheres for retrograde tracing in adult mice (Kamiyama et al. 2015). Although Kamiyama et al. made injections at C7 whereas our injections and those of Wang et al. were at C5, essentially all the key features of the distribution of retrogradely labeled CST neurons were comparable including the spatially separated clusters of neurons in the rostral sensorimotor cortex and dorsolateral cortex (S2) extending ventral and caudal to the barrel field. In all studies, these areas were separated from the main cluster of neurons in the main sensorimotor cortex by areas containing few if any labeled neurons.

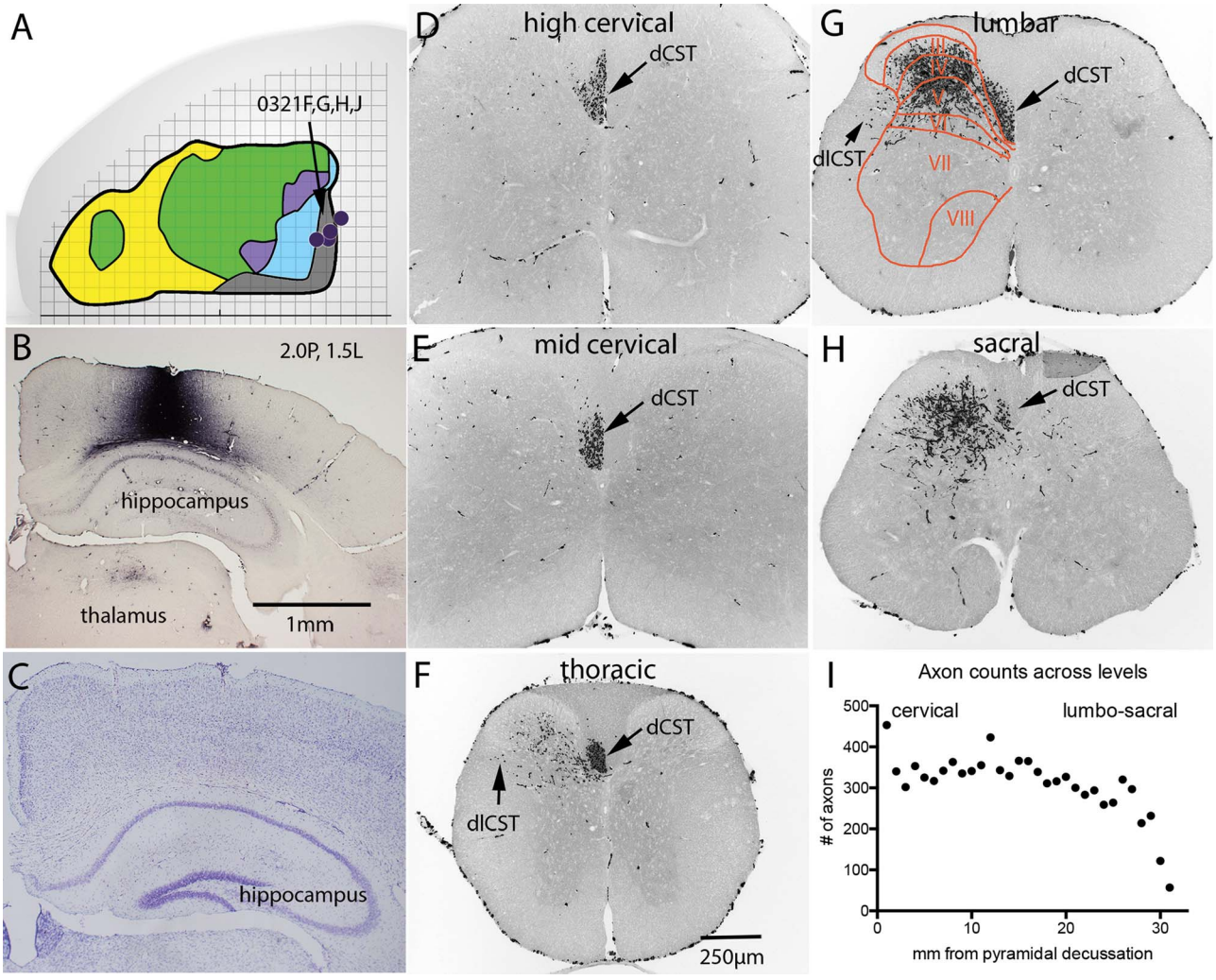

Figure 12. Caudal-most sensorimotor cortex; 1.5 mm lateral to the midline. (*A*) Map of injection sites. (*B*) BDA labeling at injection site in the case with the most labeled axons. (*C*) Cresyl violet-stained section at injection site. (*D–H*) Cy3-labeled axons at different levels following a single injection of BDA at 0.9 mm posterior and 1.1 mm lateral. Location of spinal cord laminae is indicated in *G*. Numbers in the lower part of panels *D–H* indicate distance from the pyramidal decussation. (*I*) Counts of labeled axons in the dCST in sections spaced at 1-mm interval. Abbreviations are as in Figure 5.

There was incomplete agreement among the 3 studies regarding the distribution of CST neurons that are retrogradely labeled following injections at lumbar levels (L2 spinal level in our study L4 in Kamiyama et al., and between the L4 and L5 vertebrae in Wang et al). In our study and that of Wang et al., the population of neurons that were retrogradely labeled by lumbar injections lay just caudal to the population labeled by C5 injections, with only a small area of overlap. In contrast, in Kamayama et al, there was almost complete overlap between the populations labeled following injections at C7 versus L4. The other area of disagreement is in the number of CST neurons that are double labeled following injections of different tracers at cervical versus lumbar levels. In our study, there were very few double-labeled neurons, and Wang et al. report that no double-labeled CST neurons were detected, whereas Kamiyama et al. report that considerable numbers of CST neurons are double-labeled with different fluorescent microspheres. The reasons for these discrepancy are unclear but could reflect differences in location of injection sites in the spinal cord or spread of microbeads versus AAVs along the rostro-caudal axis.

The distribution of retrogradely labeled CST neurons corresponds in general to the motor map of the mouse cortex based on microstimulation (Tennant et al. 2010) except that the motor map extends slightly beyond the boundary of the areas containing retrogradely labeled neurons and the motor map does not include the area containing CST neurons in S2. Motor maps from microstimulation (Tennant et al. 2010) show a RFA centered at about 2.0 anterior and a larger CFA, the anterior boundary of which is at around 1.0 anterior. Their microstimulation map indicates that the area between RFA and CFA represents the neck and jaw, which are served by lower motoneurons located above C5. CST projections to the motoneurons serving the neck and jaw might not extend to C5, which would account for the lack of retrograde labeling by retro-AAV or fluorogold injections at that level. We are not aware of microstimulation or optogenetic studies targeting S2 in rodents, so whether this region has motor function remains to be explored.

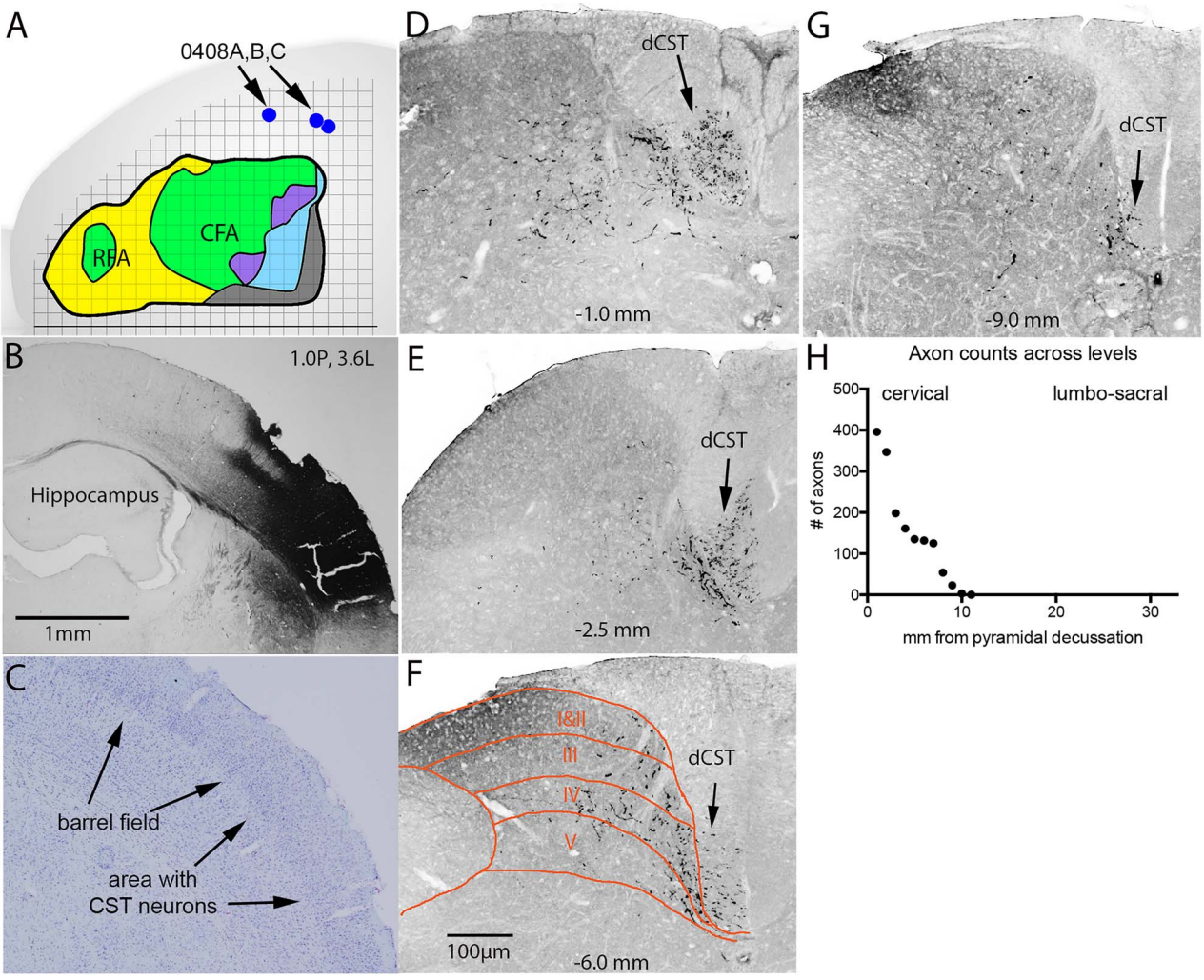

Figure 13. CST neurons in dorsolateral cortex (S2) project to high cervical levels and arborize in the medial dorsal horn. (*A*) Map of injection sites. (*B*) BDA labeling at injection site in the case with the most labeled axons. (*C*) Cresyl violet-stained section at injection site. (*D–G*) Cy3-labeled axons at different levels following a single injection of BDA at 1.0 posterior and 3.6 lateral. (*H*) Counts of labeled axons in the dCST in sections spaced at 1-mm interval. Abbreviations are as in Figure 5.

Level-Specific Projections

BDA injections into the rostral sensorimotor cortex lead to extensive labeling of arbors at cervical levels with essentially no extension beyond mid-thoracic levels. With injections into more caudal parts of the forelimb region anterior to bregma, CST axons extended further caudally in the spinal cord. Injections into the hindlimb region posterior to bregma lead to labeling of axons that extend though cervical levels in the dorsal CST largely without extending collaterals. However, injections near the forelimb/hindlimb transition just posterior to bregma led to labeling of arbors at cervical–lumbar and sometimes even sacral levels. Our findings with retro-AAV/Cre indicate that there is some overlap in the distribution of neurons that project to cervical versus lumbar levels, but the absence of extensive double labeling with injections of retro-AAV/GFP at C5 and retro-AAV/Cre at lumbar levels indicates that there are few that project to both levels. This supports conclusions from a previous study that used retro-AAVs with different fluorescent reporters (Wang et al. 2018). In addition, the fact that injections at C5 do not label neurons in the hindlimb region supports previous conclusion that there is limited uptake of retro-AAV passing through the cervical level *en route* to lumbar levels.

Our BDA injections targeting the area of the dorsolateral cortex that contains CST neurons label CST axons that terminate selectively at high cervical levels in the medial-most part of the dorsal horn. Kamiyama et al. (2015) report a similar pattern of termination in the dorsal horn at C7 with similar injections of AAV encoding fluorescent proteins. Kamiyama et al. did not report on the rostro-caudal distribution of these projections, however. Given that these projections are limited to a small area of the dorsal horn adjacent to the dorsal column, it will be of interest to determine possible motor function and/or modulation of sensory processing.

Lamina-Specific Projections

Previous studies have shown that different parts of the sensorimotor cortex project selectively to different laminae in the spinal cord. This was first shown in hamsters (Kuang and Kalil 1990) and was later confirmed in rats (Bareyre et al. 2002). For

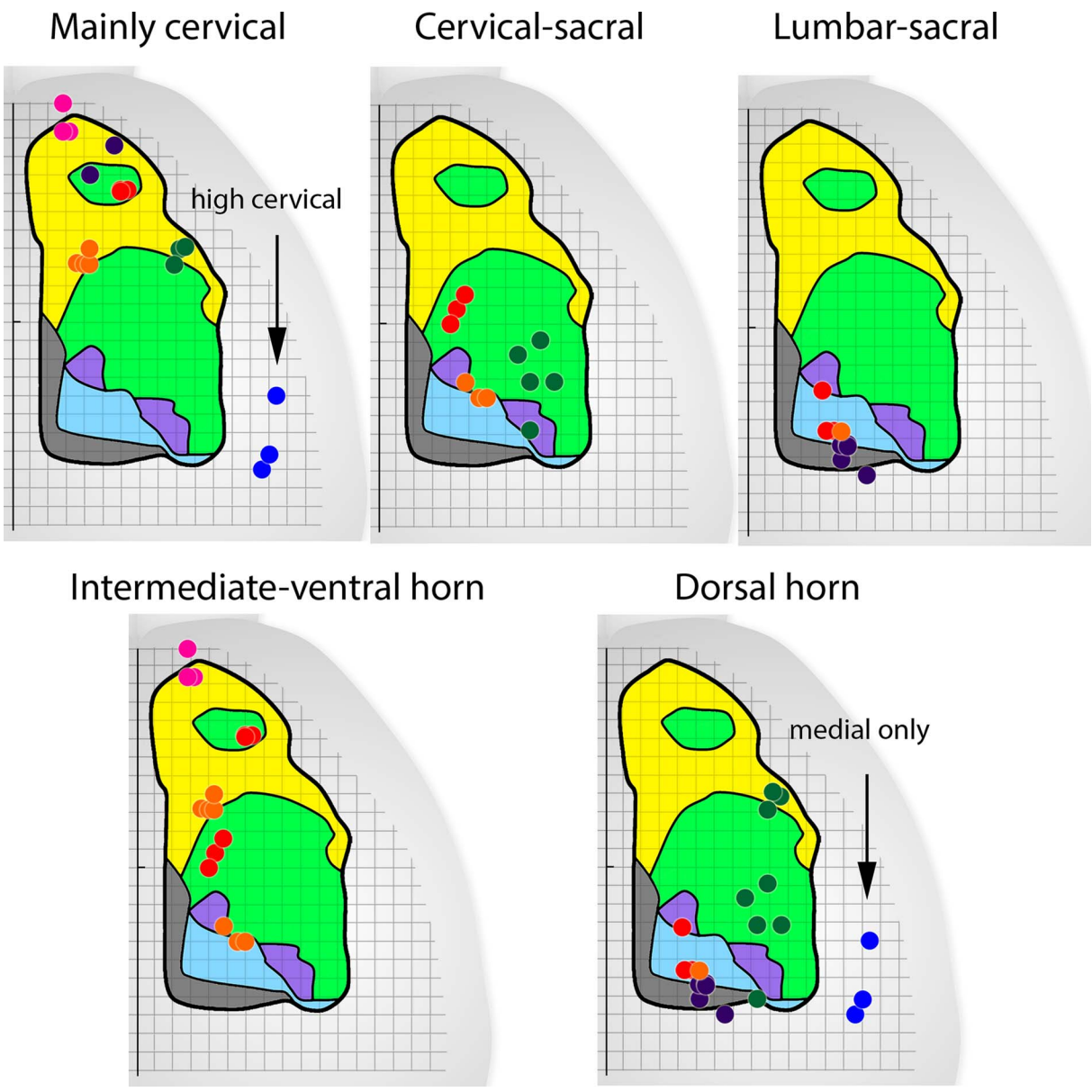

Figure 14. Summary of topographic specificity of CST projections. (*A*) Map of injection sites that give rise to CST axons that terminate mainly at cervical levels. (*B*) Map of injection sites that give rise to CST axons that terminate at cervical–sacral levels. (*C*) Map of injection sites that give rise to CST axons that extend through cervical levels without projections into the gray matter and then terminate selectively at lumbar–sacral levels. (*D*) Map of injection sites that give rise to CST axons that terminate in intermediate laminae with some axons extending into the ventral horn. (*E*) Map of injection sites that give rise to CST axons that terminate in the dorsal horn.

example, in rats, tracer injections into the "motor cortex" (2 mm anterior, 3 mm lateral) labeled CST arbors extended throughout the intermediate lamina and into the ventral horn (Bareyre et al. 2002). In contrast, following tracer injections into the "sensory cortex" (0.5 mm posterior, 4.5 mm lateral) labeled CST arbors were restricted to the dorsal horn. Kameda et al. (2019) confirm the general conclusion for mice in terms of projections to the cervical level and also provide additional granular detail on the mediolateral distribution of axon arbors in the dorsal horn at cervical levels. The present study further confirms that the rostro-medial portion of the sensorimotor cortex projects to intermediate lamina and the ventral horn and the rostro-lateral portion projects to the dorsal horn. Our results also extend the story by showing that the most posterior sensorimotor cortex projects mainly to the dorsal horn of lumbar–sacral segments with few axons extending into the ventral horn and reveal through examples that there are actually several different patterns of laminar termination based on point of origin in the cortex.

CST Arbors in the Ventral Horn

In mice, injections into the medial part of the sensorimotor cortex label CST arbors that extend into the ventral horn at cervical, lumbar, and sacral levels depending on the injection site, including into the portion of the ventral horn containing

motoneuron cell bodies and dendrites. This physical proximity does not, however, provide evidence of direct innervation of motoneurons by CST axons. Some previous studies in rats have provided evidence of direct connections (Liang et al. 1991), including extensive projections of CST axons into the cervical ventral horn and close appositions between varicosities on labeled CST axons (putative presynaptic terminals) and retrogradely labeled motoneuron dendrites (Raineteau et al. 2002). More recent physiological studies indicate that direct connections between CST axons and forelimb motoneurons exist in early postnatal rats, but that these may be transient (Maeda et al. 2016). One implication of our data is that studies to resolve this question must take into account the topographic organization of projections from different parts of the sensorimotor cortex and that extension of CST axons into the ventral horn varies by the part of the sensorimotor cortex (medial vs. lateral) and spinal level.

The Ventral CST Is Sparse in Mice

In rats, BDA injections into the sensorimotor cortex label a moderate number of axons in the ventral column ipsilateral to the injection, representing the uncrossed anterior CST that is also present in humans (Brosamle and Schwab 1997). In our previous studies in mice, however, we noted the absence of labeled axons in the ventral CST (Zheng et al. 2003; Steward et al. 2004, 2008). These previous studies assessed regenerative growth of CST axons following spinal cord injuries, and for this purpose, mice received a total of 4 BDA injections to blanket most of the sensorimotor cortex rostral and caudal to bregma. In the present study, we again found that there were no labeled axons in the ventral CST in most mice.

Our previous studies in which we did not detect ventral CST axons involved either C57Bl/6 mice or genetically modified mice with a predominantly C57Bl/6 genetic background. Previous studies of "CST-YFP" mice report YFP-labeled axons in the ventral column that disappear after bilateral pyramidotomy (Bareyre et al. 2005). CST-YFP mice are on a mixed genetic background backcrossed to C57Bl/6. Also, one previous study of regenerative growth of CST axons after dorsal hemisection injuries reports increases in the number of CST axons extending along the ventral column following spinal cord injury in mice immunized against Nogo/MAG (Sicotte et al. 2003). This study involved SJL/J mice, and CST axons were traced by injecting phytohemagglutinin-L into the sensorimotor cortex. Although it is possible that SJL/J mice have more ventral CST axons than other strains, Sicotte et al. did not show examples of labeled vCST axons in uninjured mice. This is important, because we have shown the possibility of artifactual labeling of axons following tracer (BDA) injections at early intervals after spinal cord injury (Steward et al. 2007). Indeed, this artifactual labeling occurred after dorsal hemisection injuries as used in Sicotte et al. In sum, although we cannot exclude the possibility that CST axons project via the ventral column in some strains of mice, ventral CST axons are very sparse in the strains we have tested (Balb/c, C57/BL, and transgenic mice of mixed genetic background). This is relevant for studies of motor recovery after SCI because the ventral CST is one potential source of reinnervation of caudal segments following partial injuries in rats (Weidner et al. 2001).

One other point regarding possible strain differences is that our studies with retro-AAV were in mice of mixed genetic background, whereas tract tracing was done in Balb/c mice. However, there were no evident disparities that might suggest strain differences.

Our results reinforce previous studies (Wang et al. 2018) documenting the power of retro-AAV, tissue clearing, and light sheet imaging for obtaining quantitative and complete identification of the components of the CST. Also, our data on the normal projection patterns of CST axons from different parts of the cortex to different levels and laminae of the spinal cord provide novel insights into topographic specificity of normal CST projections, which will aid in identifying differences in projection patterns in mice carrying mutations and in detecting changes in patterns of projection due to regenerative growth following injury (Hollis et al. 2016), and form part of the basis for comparisons of CST projection patterns between strains and species.

Supplementary Material

Supplementary material is available at *Cerebral Cortex* online.

Notes

Thanks to Jamie Mizufuka Dam for superb technical assistance, Kiara Quinn for help with editing videos, and Grace O'Brien and Victor Dang for assistance with quantification of axons. We gratefully acknowledge generous donations from Cure Medical and Research for Cure as well as other private donations. This study had its roots in a discussion between O.S. and Dr. J. Maclis, Harvard University about the degree to which different parts of the sensorimotor cortex in mice projected selectively to different spinal levels. *Conflict of Interest*: O.S. is a cofounder of the company "Axonis Therapeutics Inc.," which is seeking to develop therapies targeting PTEN to enable axon regeneration following injury. S.P.G. and R.A. are cofounders of the company "Translucence Biosystems, Inc.", which develops products and services for tissue clearing, imaging, and reconstruction including the Mesoscale Imaging System used in this study. Other authors declare no competing financial interests.

Funding

National Institutes of Health (grants NS047718, NS073857 to O.S.), National Institutes of Health fellowship (F31NS070558 to R.W.) and training grants (T32GM008620, EY029596 to R.A.).

References

Bareyre FM, Haudenschild B, Schwab ME. 2002. Long-lasting sprouting and gene expression changes induced by the monoclonal antibody IN-1 IN the adult spinal cord. *J Neurosci*. 22:7097–7110.

Bareyre FM, Kerschensteiner M, Misgeld T, Sanes JR. 2005. Transgenic labeling of the corticospinal tract for monitoring axonal responses to spinal cord injury. *Nat Med*. 11: 1355–1360.

Brosamle C, Schwab ME. 1997. Cells of origin, course, and termination patterns of the ventral, uncrossed component of the mature rat corticospinal tract. *J Comp Neurol*. 386: 293–303.

Dado RJ, Burstein R, Cliffer KD, Giesler GJ Jr. 1990. Evidence that Fluoro-Gold can be transported avidly through fibers of passage. *Brain Res*. 533:329–333.

Du K, Zheng S, Zhang Q, Li S, Gao X, Wang J, Jiang L, Liu K. 2015. PTEN deletion promotes regrowth of corticospinal tract axons 1 year after spinal cord injury. *J Neurosci*. 35:9754–9763.

Geoffroy CG, Lorenzana AO, Kwan JP, Lin K, Ghassemi O, Ma A, Xu N, Creger D, Liu K, He Z, et al. 2015. Effects of PTEN and Nogo codeletion on corticospinal axon sprouting and regeneration in mice. *J Neurosci*. 35:6413–6428.

Hollis ER 2nd, Ishiko N, Yu T, Lu CC, Haimovich A, Tolentino K, Richman A, Tury A, Wang S-H, Pessian M, et al. 2016. Ryk controls remapping of motor cortex during functional recovery after spinal cord injury. *Nat Neurosci*. 19:697–705.

Kameda H, Murabe N, Odagaki K, Mizukami H, Ozawa K, Sakurai M. 2019. Differential innervation within a transverse plane of spinal gray matter by sensorimotor cortices, with special reference to the somatosensory cortices. *J Comp Neurol*. 527:1401–1415.

Kamiyama T, Kameda H, Murabe N, Fukuda S, Yoshioka N, Mizukami H, Ozawa K, Sakurai M. 2015. Corticospinal tract development and spinal cord innervation differ between cervical and lumbar targets. *J Neurosci*. 35:1181–1191.

Kuang RZ, Kalil K. 1990. Branching patterns of corticospinal axon arbors in the rodent. *J Comp Neurol*. 292:585–598.

Liang FY, Moret V, Wiesendanger M, Rouiller EM. 1991. Corticomotoneuronal connections in the rat: evidence from double-labeling of motoneurons and corticospinal axon arborizations. *J Comp Neurol*. 311:356–366.

Liang H, Paxinos G, Watson C. 2011. Projections from the brain to the spinal cord in the mouse. *Brain Struct Funct*. 215:159–186.

Liu K, Lu Y, Lee JK, Samara R, Willenberg R, Sears-Kraxberger I, Tedeschi A, Park KK, Jin D, Cai B, et al. 2010. PTEN deletion enhances the regenerative ability of adult corticospinal neurons. *Nat Neurosci*. 13:1075–1081.

Maeda H, Fukuda S, Kameda H, Murabe N, Isoo N, Mizukami H, Ozawa K, Sakurai M. 2016. Corticospinal axons make direct synaptic connections with spinal motoneurons innervating forearm muscles early during postnatal development in the rat. *J Physiol*. 594:189–205.

Neafsey EJ, Sievert C. 1982. A second forelimb motor area exists in rat frontal cortex. *Brain Res*. 232:151–156.

Nielson JL, Sears-Kraxberger I, Strong MK, Wong JK, Willenberg R, Steward O. 2010. Unexpected survival of neurons of origin of the pyramidal tract after spinal cord injury. *J Neurosci*. 30:11516–11528.

Nielson JL, Strong MK, Steward O. 2011. A reassessment of whether cortical motor neurons die following spinal cord injury. *J Comp Neurol*. 519:2852–2869.

Paxinos G. 2004. *The mouse brain in stereotaxic coordinates*. Amsterdam; Boston: Elsevier Academic Press.

Preibisch S, Saalfeld S, Tomancak P. 2009. Globally optimal stitching of tiled 3D microscopic image acquisitions. *Bioinformatics*. 25:1463–1465.

Raineteau O, Fouad K, Bareyre FM, Schwab ME. 2002. Reorganization of descending motor tracts in the rat spinal cord. *Eur J Neurosci*. 16:1761–1771.

Renier N, Adams EL, Kirst C, Wu Z, Azevedo R, et al. 2016. Mapping of Brain Activity by Automated Volume Analysis of Immediate Early Genes. *Cell*. 165:1789–1802.

Sicotte M, Tsatas O, Jeong SY, Cai CQ, He Z, David S. 2003. Immunization with myelin or recombinant Nogo-66/MAG in alum promotes axon regeneration and sprouting after corticospinal tract lesions in the spinal cord. *Mol Cell Neurosci*. 23:251–263.

Steward, O, Metcalfe, M, Yee, KM, Coulibaly, A. 2016. Unexpected and unexplained accumulation of AAV vector in the pineal gland after injections into sensorimotor cortex., Society for Neuroscience, Washington, DC: Society for Neuroscience Abs.

Steward O, Zheng B, Banos K, Yee KM. 2007. Response to: Kim et al., "axon regeneration in young adult mice lacking Nogo-A/B." Neuron 38, 187-199. *Neuron*. 54:191–195.

Steward O, Zheng B, Ho C, Anderson K, Tessier-Lavigne M. 2004. The dorsolateral corticospinal tract in mice: an alternative route for corticospinal input to caudal segments following dorsal column lesions. *J Comp Neurol*. 472: 463–477.

Steward O, Zheng B, Tessier-Lavigne M, Hofstadter M, Sharp K, Yee KM. 2008. Regenerative growth of corticospinal tract axons via the ventral column after spinal cord injury in mice. *J Neurosci*. 28:6836–6847.

Tennant KA, Adkins DL, Donlan NA, Asay AL, Thomas N, Kleim JA, Jones TA. 2010. The organization of the forelimb representation of the C57BL/6 mouse motor cortex as defined by intracortical microstimulation and cytoarchitecture. *Cereb Cortex*. 21:865–876.

Wang Z, Maunze B, Wang Y, Tsoulfas P, Blackmore MG. 2018. Global connectivity and function of descending spinal input revealed by 3D microscopy and retrograde transduction. *J Neurosci*. 38:10566–10581.

Wang Z, Reynolds A, Kirry A, Nienhaus C, Blackmore MG. 2015. Overexpression of Sox11 promotes corticospinal tract regeneration after spinal injury while interfering with functional recovery. *J Neurosci*. 35:3139–3145.

Weidner N, Ner A, Salimi N, Tuszynski MH. 2001. Spontaneous corticospinal axonal plasticity and functional recovery after adult central nervous system injury. *Proc Natl Acad Sci U S A*. 98:3513–3518.

Zheng B, Ho C, Li S, Keirstead H, Steward O, Tessier-Lavigne M. 2003. Lack of enhanced spinal regeneration in Nogo-deficient mice. *Neuron*. 38:213–224.

Zheng B, Lee JK, Xie F. 2006. Genetic mouse models for studying inhibitors of spinal axon regeneration. *Trends Neurosci*. 29:640–646.